Report Date: October 30, 2002

Semi Annual Technical Progress Report

INVESTIGATION OF EFFICIENCY IMPROVEMENTS DURING CO_2 INJECTION IN HYDRAULICALLY AND NATURALLY FRACTURED RESERVOIRS

DOE Contract No.: DE-FC26-01BC15361

Harold Vance Department of Petroleum Engineering
Texas A& M University
3116 TAMU
College Station, TX 77843-3116
(979) 845-2241

Contract Date:	September 28, 2001
Anticipated Completion Date:	September 27, 2004
Principal Investigator:	David S. Schechter Harold Vance Department of Petroleum Engineering
Contracting Officer's Representative:	Dan Ferguson National Petroleum Technology Office
Report Period:	March 27, 2002- September 27, 2002

DISCLAIMER

ABSTRACT

The objective of this project is to perform unique laboratory experiments with artificial fractured cores (AFCs) and X-ray CT to examine the physical mechanisms of bypassing in HFR and NFR that eventually result in less efficient CO_2 flooding in heterogeneous or fracture-dominated reservoirs. This report provides results of the second semi-annual technical progress report that consists of three different topics.

In the first topic, laboratory experiments were performed on a Berea core to investigate the changes in rock properties and fluid flow under different stress-state conditions. A comparative study of different stress conditions was also conducted to analyze the effect of the various loading systems. The experimental results show that fracture permeability reduces significantly as the stress increases compared to matrix permeability. The hydrostatic and triaxial stresses have greater impacts on permeability reduction compared to applying stress in the uniaxial stress condition. Fracture flow dominates when the applied stress is less, however, the matrix flow rate increases as applied stress increases and dominates at high stress even if the fracture does not heal completely.

In the second topic, the preliminary results of static imbibition experiments are presented as a precursor to image the saturation profiles using X-Ray CT scanner. The static and dynamic imbibition experiments have been done previously (Schechter *et al*, 2002). The imaging of imbibition experiment is underway to track the saturation profiles using X-ray CT scanner. Hence, no more conclusions are drawn from this study at this time.

In the last topic, the modeling of fluid flow through a single fracture incorporating the effect of surface roughness is conducted. Fracture permeability is usually estimated by a cubic law that is based on the theory of hydrodynamics for the laminar flow between flat plates. However, the cubic law is too simple to estimate the fracture permeability correctly, because the surface of real fracture is much more complicated and rougher than the surface of flat plate. Several researchers have shown that the flow characteristics of an actual fracture surface would be quite different due to the effect of tortuosity, impact of surface roughness and contact areas. Nonetheless, to date, these efforts have not converged to form a unified definition on the fracture aperture needed in the cubic law. In this study, therefore, we show that the cubic law could still be used to model small-scale and field-scale data as long as it is modeled effectively, accounting for the effect of surface roughness associated with the fracture surface. The goal of this research is to examine the effect of surface roughness for flow through fractures and to effectively incorporate them into simulations with the aid of geostatistics. Since the research has been supported with experimental results, the consistency of the results enabled us to define a methodology for single fracture simulation. This methodology successfully modeled the flow rate and pressure drop from fractured core experiments, which were earlier not possible through parallel plate approach. Observations suggest that the fracture aperture needs to be distributed to accurately model the experimental results. The effect of friction and tortuosity due to surface roughness needs to be taken into account while modeling.

TABLE OF CONTENTS

LIST OF TABLES

LIST OF FIGURES

I. Investigating The Changes In Matrix and Fracture Properties And Fluid Flow Under Different Stress-state Conditions

1.1 Introduction

The main objective of this study is to analyze the variation of permeability with the effective stress. Uniaxial, triaxial and hydrostatic laboratory experiments were conducted to study the effect of confining pressure on permeability in both the unfractured and fractured cores. Various works have been done in the past in investigating the effect of confining stress on the core samples. The literature review is divided into three parts. The first part deals with the study of permeability changes with uniaxial stress. The review is further extended to include the triaxial and hydrostatic effects on permeability. The later part of the review deals with the experimental study of fracture permeability variations with the effective stress.

Fatt and Davis (1952) observed a reduction in permeability with an overburden pressure. The permeabilities of eight cores were plotted as a function of the overburden pressure. They observed that a significant decrease in permeability of the sandstones occurs at an overburden pressure range of zero to 3000 psi. McLatchie *et al* (1958) determined oil permeability of core material under various overburden loads from zero to 8000 psi. He concluded that the shaly cores have a greater percentage of reduction in permeability compared to the changes in permeability of the clean sands. Wyble (1958) used kerosene to apply a radial pressure of zero to 5000 psi to the cylindrical cores while axial stresses were at atmospheric. He observed that even though the pressurizing system is changed, the results still are consistent with the observations by Fatt (1953). Dobrynin (1962) observed changes in physical properties with the overburden pressure. The permeability at room temperature was calculated using nitrogen as the flowing medium. He used two series of measurements, one with internal pore pressure equal to the

atmospheric pressure, while the overburden pressure ranged from zero to 20,000 psi, and the other with an internal pore pressure of 1800 psi. He found that on the basis of net overburden pressure there was practically no difference between these two sandstones. He also assumed that the changes in permeability under pressure depend mainly upon the contraction of the pore channels.

Bergamini (1962) studied the effects of non-uniform stress on the permeability of sandstones by applying radial confining pressure and axial stress independent of each other. At first, tests were run with radial and axial stresses applied equally (hydrostatic loading) and then the axial stress was kept constant while the radial pressure was increased. Permeabilities were measured up to 4000 psi. The reduction of permeability of the order of 10 percent was observed for most of the sandstones. Gray *et al* (1963) showed that the permeability reduction of cylindrical samples of two sandstones, when subjected to mechanical stress, is a function of the ratio of radial to axial stress. The axial stress was only one-third of the applied radial stress. Wilhelmi *et al* (1967) conducted tests on three outcrop sandstones at several confining pressures and axial stresses up to approximately 80 percent of failure stress. He observed that greater reduction in permeability occurred in hydrostatic loading but substantial reduction did occur upon application of deviator (triaxial) stress. The deviator stress is $\sigma_y - \sigma_x$, where σ_y is the axial stress and $\sigma_x = \sigma_z$, is the lateral stress. The reductions were of the order of 10 to 20 percent for Berea sandstone. Morita *et al* (1984) conducted triaxial failure tests on berea cores and measured both vertical and horizontal permeabilities. The permeabilities decreased initially during axial loading but increased again close to the failure because of the dilation behavior of the rock. Holt (1990) conducted triaxial compression and extension tests on Triassic sandstone. He observed that the single phase permeability decreased rapidly at non hydrostatic stress conditions when the shear stress $[1/2(|\sigma_{max} - \sigma_{min}|)]$ exceeded the yield level. Keaney *et al* (1998) introduced a newly developed single-ended transient pulse permeability measurement technique coupled to a high pressure triaxial deformation apparatus. The technique was applied to Tennessee sandstone and has demonstrated the dependency of complex interplay between hydrostatic and non hydrostatic stresses. It was found that while performing the triaxial

deformation experiments, the permeability decreased because of compaction, but close to failure the permeability is increased due to dilation.

Hubbert *et al* (1957) showed that the fractures were formed perpendicular to the least principal stress. Jones (1975) studied the effects of confining pressure on fracture flow in carbonate rocks. He used uniform triaxial compressive loading up to 20,000 psi. The fractures were fabricated and blocked by sandwiching with thin gum rubber. He calculated the effective fracture clearance assuming the fractures to be parallel plate. He concluded that fracture permeability is greatly reduced by increasing the confining pressure. The fracture permeability behavior governed at lower confining pressures and matrix permeability behavior governed at higher confining pressures. The fracture does not heal completely even at 20,000 psi. Also the behavior of fractures in limestone, dolomite and marble is sufficiently similar to be represented by the same expression. Teufel *et al* (1993) made a case study of the Ekofisk field, which is a naturally fractured chalk reservoir. Permeability was measured during hydrostatic and triaxial compression tests on cylindrical samples that had a single, sub-planar fracture. He applied stress paths of K ($\Delta\sigma_{Hmin}/\Delta\sigma_v$) = 1.0, 0.5 and 0.2 on the loading tests. He found that under hydrostatic loading, the permeability of unfilled fractures reduced greatly than the partially filled fracture. Also the stress path of k = 1.0 (hydrostatic) will have maximum reduction in permeability.

No research has been carried out to quantify the fracture aperture and permeability of fractures so far. The change in effective permeability of fractures and matrix has been studied in detail under different effective stress, but deriving the permeability from the effective permeability to study the permeability of fracture alone has not been considered. Also there is no work involved in the study of matrix and fracture flowrates under different stress-state conditions. Hence our research extended the previous work by investigating the changes in matrix and fracture permeabilities, fracture aperture, matrix and fracture flowrates under different stress-state conditions (uniaxial, triaxial and hydrostatic stresses). The results of the uniaxial stress experiment have been provided in the earlier report (Putra *et al*, 2002). This report mainly discusses detail about

triaxial and hydrostatic experiments and the comparison between the results of uniaxial, triaxial and hydrostatic experiments.

1.2 Hydrostatic Stress Experiments

1.2.1 Experimental Description

The core sample is subjected to both overburden pressure and axial stress. The axial stress is equal to the overburden pressure for the hydrostatic experiment. Permeability is evaluated at various confining pressures and at various injection rates. The cores are then fractured subsequently and the effective permeability due to fractures is evaluated at various confining pressures and injection rates. The parameters are plotted against overburden pressure to study the effect of confining stress.

1.2.2 Berea cores

Berea sandstone was used in this study. Berea sandstone was selected because it is widely used as a standard porous rock for the experimental work in the petroleum industry. The cylindrical core sample was cut from 0.5 ft^3 blocks of Berea sandstone. The diameter of the sample is 3.6 cm. The length of the core is 4.88 cm. The dimensions are the average values of 3 to 4 measurements using a vernier caliper. The bulk volume of the sample is 49.68 cc.

1.2.3 Brine composition

Synthetic brine was used in the experiments. It was prepared by dissolving Nacl and $CaCl_2.2H_2O$ in distilled water. The brine compositions are shown in Table 1.1.

1.2.4 Pore Volume and Porosity

The porosity is calculated by the saturation method. The saturation method of determining porosity consists of saturating a clean dry sample with a fluid of known density and determining the pore volume from the gain in the weight of the sample. For this experiment, the core is saturated with brine. The pore volume is calculated from the following expression

$$PV = \frac{W_{wet} - W_{dry}}{\rho_b}$$

Where W_{dry} is the weight of the dry core, W_{wet} is the weight of the core after saturating with brine and ρ_b is the density of the brine. The pore volume was calculated to be 11.71 cc.

Porosity is calculated as a percentage from the following expression

$$\phi = \frac{PV}{BV} * 100$$

The calculated porosity is 23.58%.

1.3 Experimental Procedures

1.3.1 Core Saturation

Dry core samples were weighed on a balance. The core sample was then saturated with deaerated brine using a vacuum pump for at least 12 hours. After saturating the core samples with brine, a period of 3 days was allowed for the brine to achieve ionic equilibrium with the rock.

1.3.2 Core Flooding

The saturated core is inserted in the Hassler-Type core holder. Overburden pressure is applied in the radial direction and the axial tension is applied along the axis of the Berea core, perpendicular to the overburden pressure. An initial overburden pressure of 500 psi is applied. This is followed by core flooding with the brine solution at flow rates of 5, 10, 15 and 20cc/min. The pressure drop across the core is recorded in the transducer. The experiments are repeated for overburden pressures of 1000 psi and 1500 psi and the corresponding pressure drops are recorded. Subsequently, the core is fractured along the axis and the experiment is repeated as before for the fractured core. The experiment can be performed for the two-phase flows as shown in the figure (Fig.1.1). However, the focus is on the single-phase flow.

1.4 Discussion of Experimental Results

1.4.1 Effect of hydrostatic stress on the permeability

Permeability of the rock decreases with the increase in the applied stress. Fig. 1.2 shows the effect of overburden pressure on permeability of both the unfractured and the fractured core. The permeability is reduced in both the cases with the increase in the stress level; however the decrease in permeability of the unfractured core is very less compared to the fractured core.

The resistance to fluid flow in fractures is less compared to the matrix. The fluid, therefore, tends to take the preferential path of the fractures rather than flowing through the matrix. Because of this reason, the effective permeability of the fractured core is higher than the matrix permeability. The increase in the hydrostatic stress tends to close the fractures and increase the resistance to fluid flow. Hence the effective permeability of the fractured core reduces greatly with the increase in the hydrostatic stress. The effective permeability of the fractured core will be close to the matrix permeability at higher hydrostatic stress, but there will be some effect of fractures. This is because the fractures are not completely healed even at a higher stress. Hence there will be a residual effect of fractures on the effective permeability of the core as is evident from Fig. 1.3. The normalized permeability of both the unfractured and fractured core is plotted against overburden pressure at a flowrate of 5 cc/min.

1.4.2 Effect of hydrostatic stress on the fracture aperture

The fracture aperture is the width between the fracture surfaces. The fracture aperture is not uniform along the fractures and depends on the roughness of the fracture surfaces. If the fracture surface roughness is high, there will be more variations in the aperture. The aperture will be maximum at some points and minimum at other points. Hence the fracture permeability depends upon the fracture aperture distributions and the conductivity of the fractures. Since the fracture aperture is not uniform, it is very difficult to quantify fracture aperture at all points of the fracture path experimentally. Hence the assumption of parallel plate is used for calculating the mean fracture aperture. The formula for calculating the fracture aperture using the above assumption is presented

in the earlier report (Putra, 2002). The fracture aperture also depends upon the physical properties of the core and also depends on the size of the core sample. The matrix permeability and the effective fracture permeability greatly influences the calculation of the mean fracture aperture.

The fracture aperture is calculated for different hydrostatic stress and flowrates. If the hydrostatic stress increases then the effective fracture permeability and fracture aperture decrease significantly. The fracture aperture is more dependent on the effective fracture permeability than on matrix permeability since the variations of the matrix permeability with increase in hydrostatic stress are less compared to the effective fracture permeability. The fracture aperture is almost insensitive to the increase in the injection rate. Fig. 1.4 shows the plot of fracture aperture against overburden pressure.

1.4.3 Effect of hydrostatic stress on the fracture permeability

The fracture permeability determination is based on the fracture aperture. The fracture permeability is defined as the conductivity of the fractures to the fluid flow in the fractured core. The effective permeability due to fractures is the combination of both fracture permeability and matrix permeability. The fracture permeability is calculated assuming the flow of fluid between the parallel plates. The fracture permeability is proportional to the square of the fracture aperture by combining the viscous and the Darcy equation for flow. Usually the fracture permeability is very high compared to the matrix permeability; and hence, the fluid tends to flow through the fracture with relative ease compared to the matrix. However, the fracture permeability decreases significantly with the increase in the hydrostatic stress. Figure 1.5 shows the variations of fracture permeability with the increase in the hydrostatic stress.

1.4.4 Effect of hydrostatic stress on the fracture and matrix flow rates

The fracture flowrate depends on the fracture permeability and the fracture aperture. The fluid flow in fracture and the matrix depends on the injection rate. The fluid will rush in the fractures since the fracture permeability is high compared to the matrix. But the volumetric rate of the fracture region is small compared to the matrix block,

hence, some of the fluid diverts to matrix block. The flowrate through the fracture depends on the fracture permeability and fracture aperture. If the hydrostatic stress increases, the fracture permeability and aperture decrease, which also decreases the volumetric rate of the fracture region. Therefore at high hydrostatic stress, the fluid flow is not dominant in the fracture anymore although some amount of the flow still occurs due to the non-healing nature of the fractures as presented in Figs. 1.6 and 1.7.

1.5 Triaxial Stress Experiments

1.5.1 Experimental Description

The core sample is subjected to both overburden pressure and axial stress. The axial stress is kept at one-third of the overburden pressure for the triaxial experiment. Matrix permeability is evaluated at various confining pressures and at various injection rates. The cores are then fractured subsequently and the effective permeability due to fractures is evaluated at various confining pressures and injection rates. The parameters are plotted against overburden pressure to study the effect of confining stress.

1.5.2 Berea cores

Berea sandstone was used in this study. The diameter of the sample is 3.59664 cm. The length of the core is 5.047 cm. The dimensions are the average values of 3 to 4 measurements using a vernier caliper. The bulk volume of the sample is 53.23 cc. The pore volume and porosity are calculated as discussed before under hydrostatic loading. The pore volume is calculated as 12.55 cc and porosity is calculated as 23.58%. The core saturation was carried out as explained before under hydrostatic loading.

1.5.3 Core Flooding

The saturated core sample is inserted in the Hassler-Type core holder. The axial stress is kept one-third of the overburden pressure for the triaxial experiment. Overburden pressure is applied in the radial direction and axial tension is applied along the axis of the Berea core, perpendicular to the overburden pressure. An initial overburden pressure of 500 psi is applied. This is followed by core flooding with the brine solution at flow rates

of 5, 10, 15 and 20cc/min. The pressure drop across the core is recorded in the transducer. The experiments are repeated for overburden pressures of 1000 psi and 1500 psi and the corresponding pressure drops are recorded. Subsequently, the core is fractured along the axis and the experiment is repeated as before for the fractured core. The experiment can be performed for the two-phase flows as shown in the Fig. 1.8. However, the focus for these experiments is on the single-phase flow.

1.6 Discussion of Experimental Results

1.6.1 Effect of triaxial stress on the permeability

Permeability of the rock decreases with the increase in the applied stress. Fig. 1.9 shows the effect of overburden pressure on permeability of both the unfractured and the fractured core. The permeability is reduced in both cases by an increase in stress level; however, the decrease in permeability of the unfractured core is much less compared to the fractured core.

The increase in the triaxial stress tends to close the fractures and increase the resistance to fluid flow. Hence the effective permeability of the fractured core decreases significantly with the increase in triaxial stress. At 1500 psia, the effective permeability of the fractured core converges to matrix permeability due to the closing of fracture aperture. Figure 1.10 shows that the matrix permeability decreases about 20% from its initial permeability compare to 80% permeability reduction of fractured core at the same triaxial stress.

1.6.2 Effect of triaxial stress on the fracture aperture

The fracture aperture is calculated for different triaxial stress and flowrates. If the triaxial stress increases then the effective fracture permeability and fracture aperture decrease significantly, which is a similar response to previously applied stresses (uniaxial and hydrostatic stresses). Again it shows that the fracture aperture is almost insensitive to

the increase in the injection rate. Fig. 1.11 shows the plot of fracture aperture against overburden pressure.

1.6.3 Effect of applied stress on the fracture permeability

The fracture permeability determination is based on the fracture aperture. However, the fracture permeability decreases greatly with the increase in the triaxial stress. Fig. 1.12 shows the variations of fracture permeability with the increase in triaxial stress.

1.6.4 Effect of applied stress on the fracture flow rate

The fracture flowrate depends on the fracture permeability and the fracture aperture. The rate of flow through the fracture depends on the fracture permeability and fracture aperture. If the triaxial stress increases, the fracture region becomes small and the flow of the fluid is not dominant in the fracture, although some amount of the flow occurs due to the non-healing nature of the fractures. Hence, the fracture flowrate decreases with increase in the triaxial stress. Fig. 1.13 shows the plot of fracture flowrate against overburden pressure at various flowrates.

1.6.5 Effect of applied stress on the matrix flow rate

The matrix flowrate depends on the matrix permeability and the fracture aperture. The presence of a fracture reduces the flow through the matrix because the resistance is least in the fracture. However the increase of triaxial stress closes the fracture aperture and hence the matrix flowrate dominates. Fig. 1.14 shows the plot between matrix flowrate and the overburden pressure at various injection rates.

1.7 Comparison of Uniaxial, Triaxial and Hydrostatic Results

1.7.1 Effect of applied stress on permeability of an unfractured core

As mentioned earlier that permeability of the core reduces with the increase in the applied stress. Three types of applied stress used in our experiments are uniaxial, triaxial and hydrostatic stresses. The difference between those stresses is illustrated in Fig. 1.15. The uniaxial stress has uniform stress around the body of the core (confining stress), but no axial stress applied in the axis of the core. The triaxial stress has the confining stress and also has an axial stress applied along the axis of the core. The axial stress is kept one-third of the confining stress. The hydrostatic stress has uniform confining and axial stresses. Figure 1.16 shows clearly that hydrostatic stress has the highest impact on permeability reduction followed by triaxial and uniaxial stresses. The permeabilities are normalized and plotted against overburden pressure for the comparison of the results.

1.7.2 Effect of applied stress on permeability of fractured core

The permeability of the fractured core decreases with the increase in the applied stress. As discussed in the previous section, the reduction in permeability is more in case of hydrostatic stress since the applied stress is more than that of triaxial condition. Figure 1.17 is the plot between the normalized effective permeability due to fracture against overburden pressure. The reduction in the effective permeability due to fracture is more than the reduction in the matrix permeability in the unfractured core. The residual effects of the fracture at higher pressure are due to the fact that the fracture does not heal completely even at higher stress.

1.7.3 Effect of applied stress on fracture aperture

The fracture aperture greatly depends on the applied stress. The fracture aperture variation depends on the fracturing technique. In the laboratory, the cores are fractured using a hydraulic cutter. The fracture aperture depends on the load applied on the core while cutting. The usual trend is that the fracture aperture decreases significantly with the increase in the applied stress. Figure 1.18 is the plot between fracture aperture and the

overburden pressure for a flowrate of 5cc/min. There is not much difference between the hydrostatic and triaxial stress conditions.

1.7.4 Effect of overburden pressure on fracture permeability

The fracture permeability depends on the fracture aperture. The fracture permeability decreases greatly with the increase in the applied stress. Figure 1.19 is the plot between the overburden pressure and the fracture permeability.

1.8 Conclusions

1. The absolute permeability decreases with the increase in hydrostatic stresses.
2. The reduction of effective permeability due to fractures with applied stress is more compared to the unfractured core.
3. The fracture aperture and fracture permeability decreases with an increase in the applied stress.
4. Fracture flow dominates when the applied stress is less; however, the matrix flow rate increases as applied stress increases and dominates at high stress even if the fracture does not heal completely.
5. The hydrostatic stress has the greatest impact on reduction the matrix and fracture permeabilities and fracture aperture followed by the triaxial and uniaxial stresses.

1.9 References

1. Fatt, I and Davis, D. H: "Reduction in Permeability with Overburden Pressure", *Trans.,* AIME (1952) **195**, 329.
2. Fatt, I: "The Effect of Overburden Pressure on Relative Permeability", *Trans.*, AIME (1953) **195**, 329.
3. Mc Latchie, A. S., Hemstock, R. A. and Young, J. W: " The effective Compressibility of Reservoir Rock and Its Effects on Permeability", *Trans.*, AIME (1958) **213**, 386-388.

4. Wyble, D. O: "Effect of Applied Pressure on Conductivity, Porosity and Permeability of Sandstones", *Trans.*, AIME (1958) **231**, 430-432.
5. Dobrynin, V. M: "The Effect of Overburden Pressure on Some Properties of Sandstones", *SPEJ* (Dec 1962) 360-366.
6. Bergamini, G: "The Effect of Non-Uniform Stress on Permeability of Sandstones", Unpublished report, U. of California. Petroleum Engineering Laboratory (May 1962).
7. Gray, D. H., Fatt, I., and Bergamini, G.: "The Effect of Stress on Permeability of Sandstone Cores", *SPEJ* (June 1963) 95-100.
8. Wilhelmi, B. and Somerton, W. H: "Simultaneous Measurement of Pore and Elastic Properties of Rocks Under Triaxial Stress Conditions", paper SPE 1706 (1967).
9. Morita, N. *et al.:* "Rock Property Change During Reservoir Compaction," paper SPE 13059 presented at the 1984 SPE Annual Technical Conference and Exhibition, Houston, Sept. 16-19.
10. Holt, R. M: "Permeability Reduction Induced by a Nonhydrostatic Stress Field", SPE 19595, Presented at the 64th Annual Technical Conference and Exhibition of SPE in San Antonio, TX (1989), 251-258.
11. Keaney, G. M. J., Meredith, P. G. and Murrell, S. A. F: "Laboratory Study of Permeability Evolution in'Tight' Sandstone under Non-Hydrostatic Stress Conditions", SPE/ISRM 47265, presented at the SPE/ISRM Eurock '98 held in Trondheim, Norway, 8-10 July 1998.
12. Hubbert, M. K. and Willis, D.G: "Mechanics of Hydraulic Fracturing", *Trans.*, AIME (1957) **210**, 153-168.
13. Jones, F. O: "A Laboratory Study of the Effects of Confining Pressure on Fracture Flow and Storage Capacity in Carbonate Rocks", SPE 4569, (1975).
14. Teufel, L. W., Rhett, D. W, Farrell, H. E. and Lorenz, J. C.: "Control of Fractured Reservoir Permeability by Spatial and Temporal Variations in Stress Magnitude and Orientation", SPE 26437, presented at the 1993 Annual Technical Conference and Exhibition of SPE in Houston, TX.
15. Putra, E.: "Effect of Overburden Pressure on Unfractured and Fractured Permeability Cores," Semi-Annual Report (DOE Contract No.: DE-FC26-01BC15361), Oct 2001-March 2002.

Table 1.1- Synthetic Brine Composition

Salts Content	Concentrations (mg/L)
Nacl	122,699
$CaCl_2.2H_2O$	7,497
Total Dissolved Solids	130,196

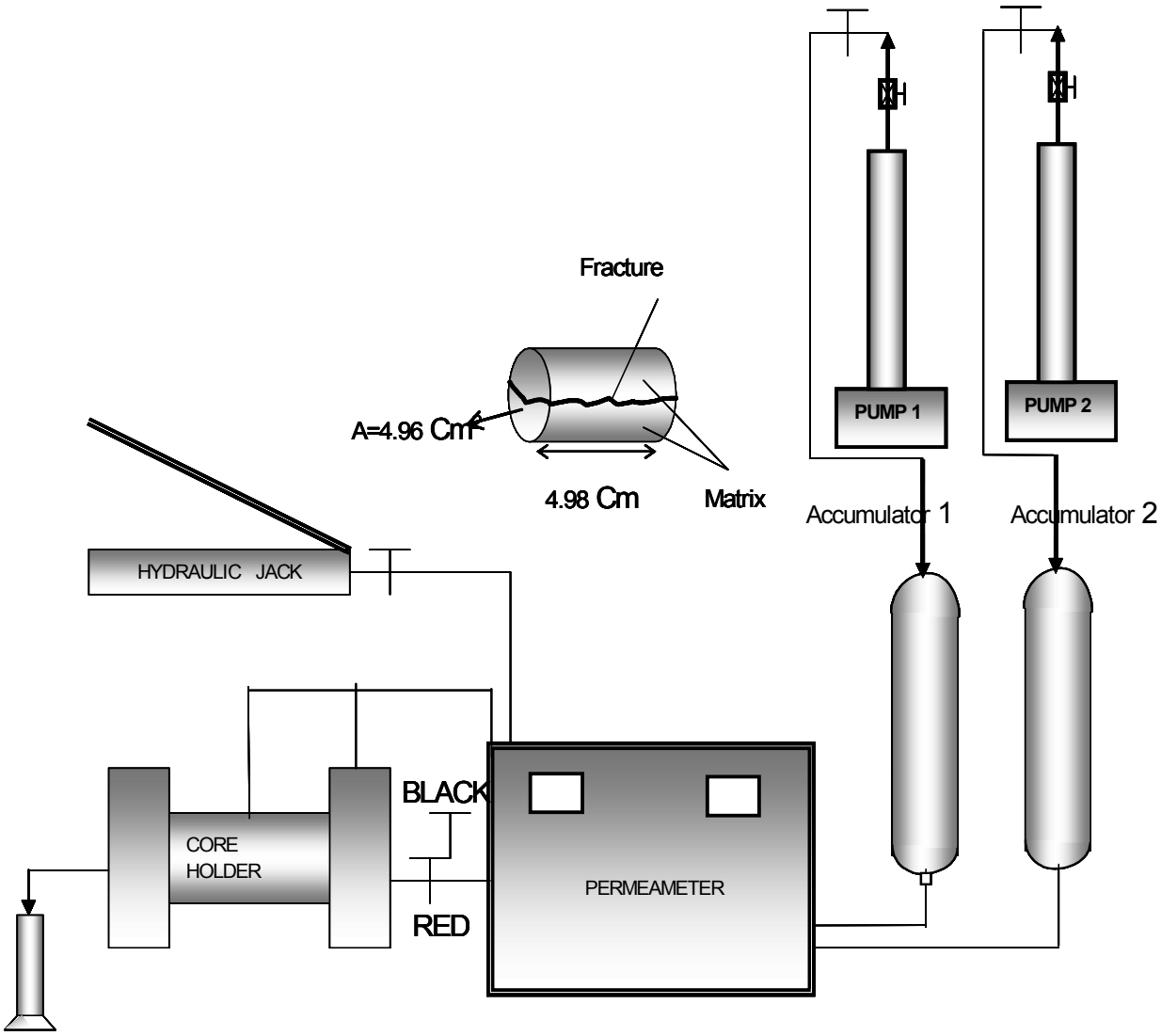

Fig. 1.1 - Hydrostatic Loading Apparatus

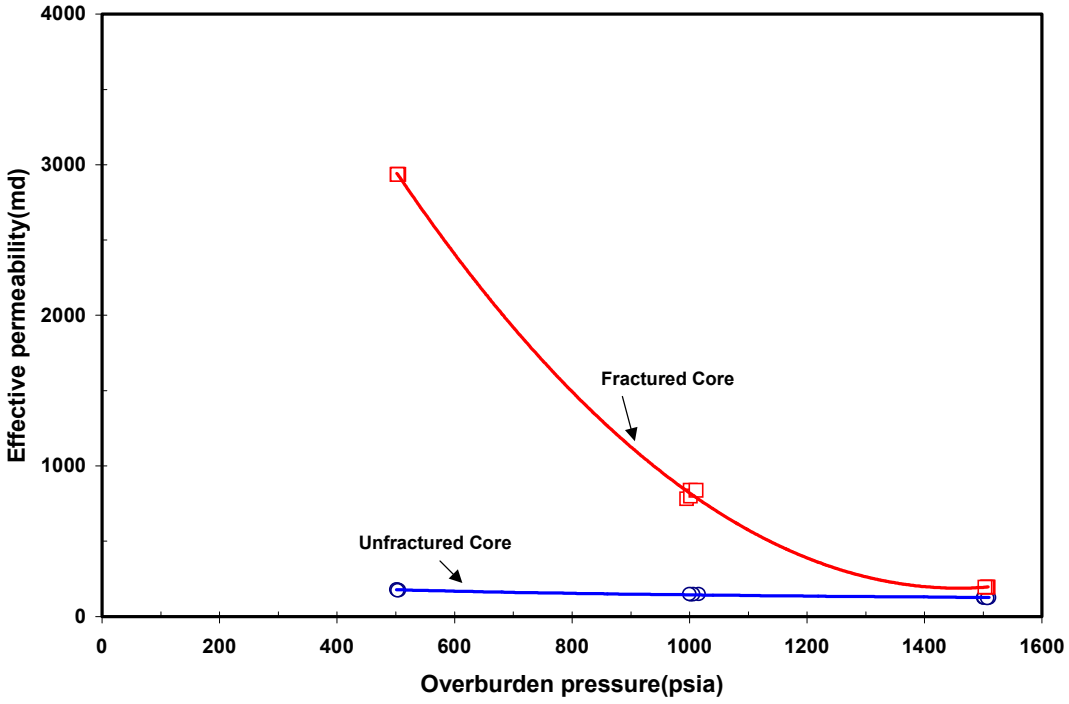

Fig. 1.2 – Permeability reduction due to hydrostatic stress

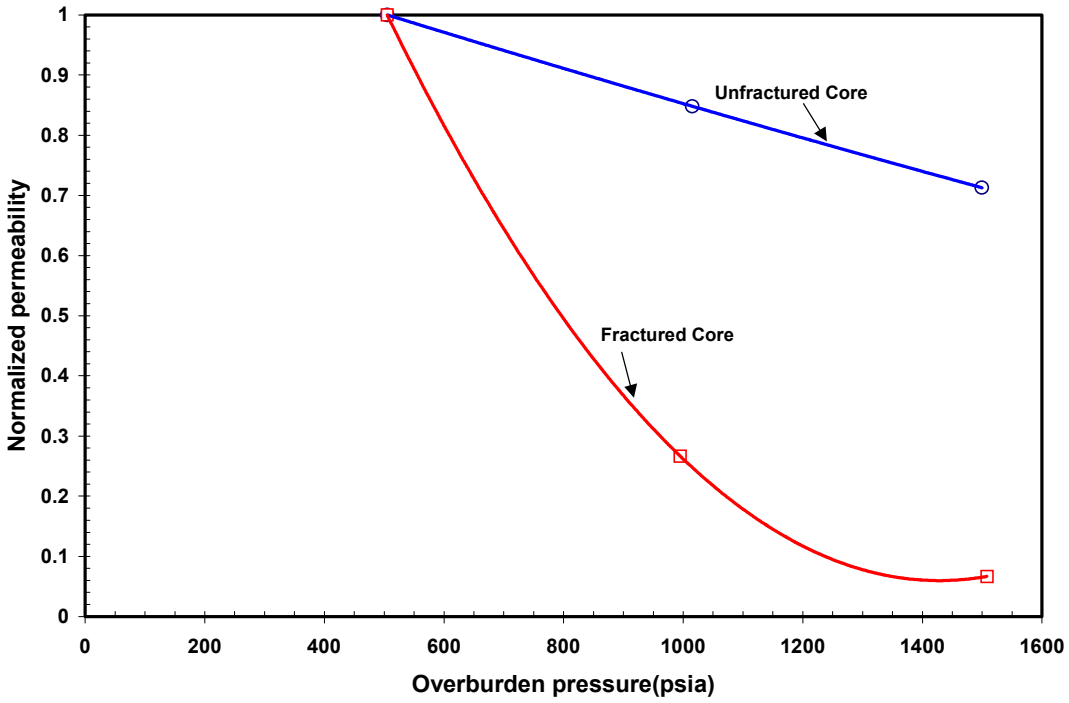

Fig. 1.3 – Normalization permeability reduction due to hydrostatic stress at injection 5 cc/min

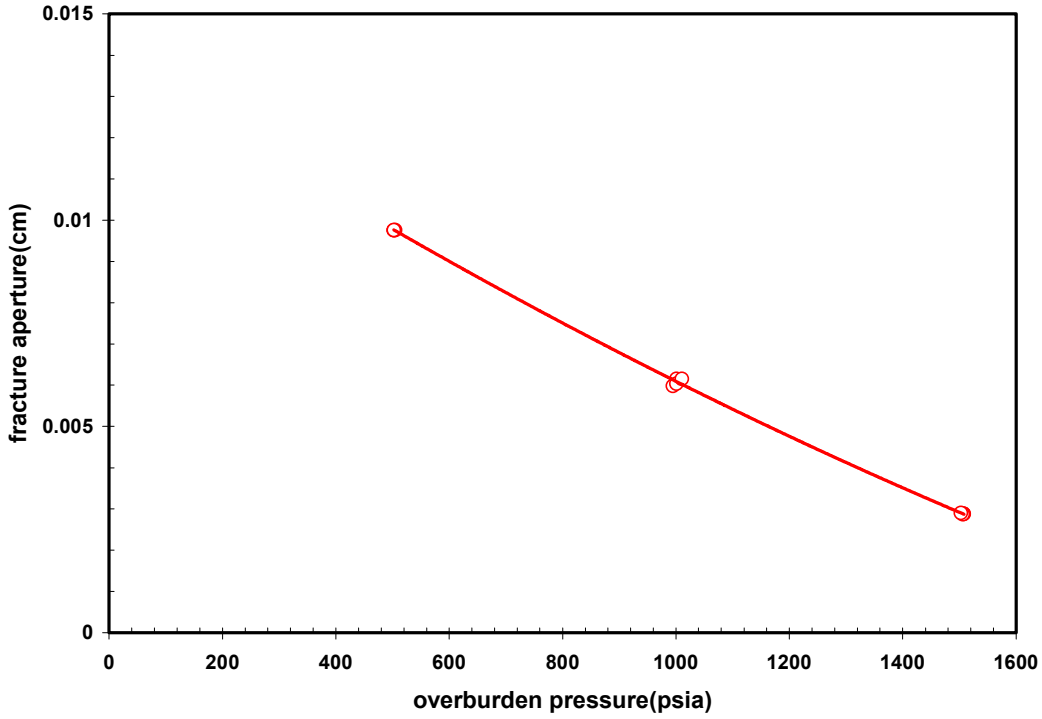

Fig. 1.4 – Fracture aperture reduction due to hydrostatic stress

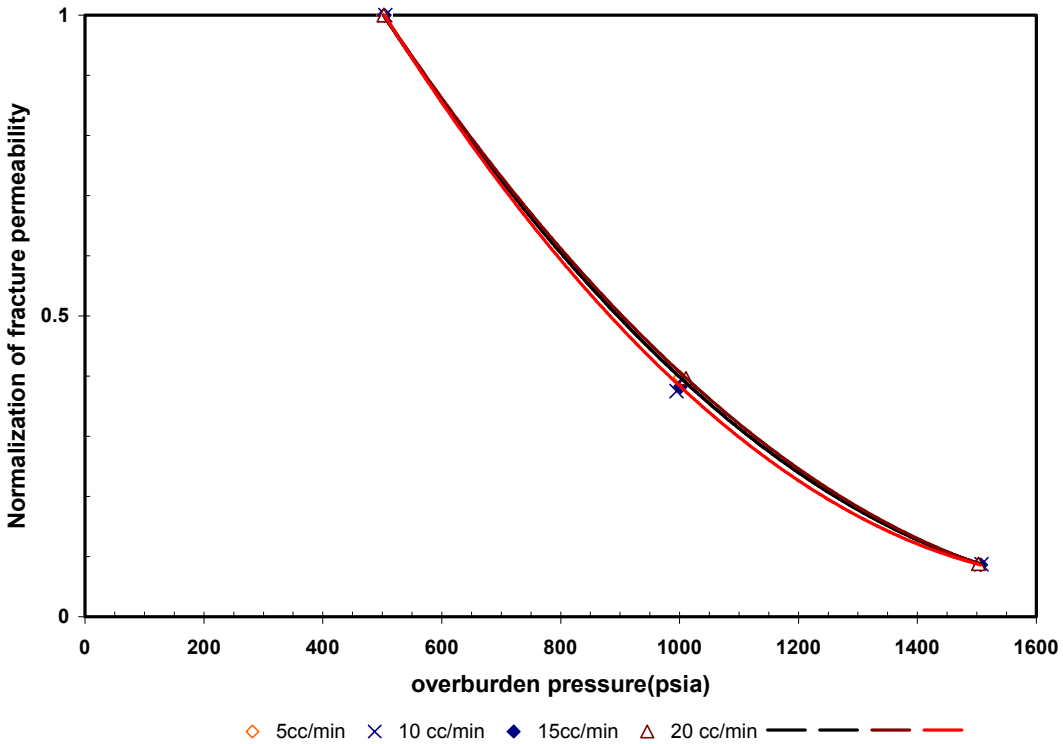

Fig. 1.5 – Fracture permeability reduction due to hydrostatic stress at different injection rate

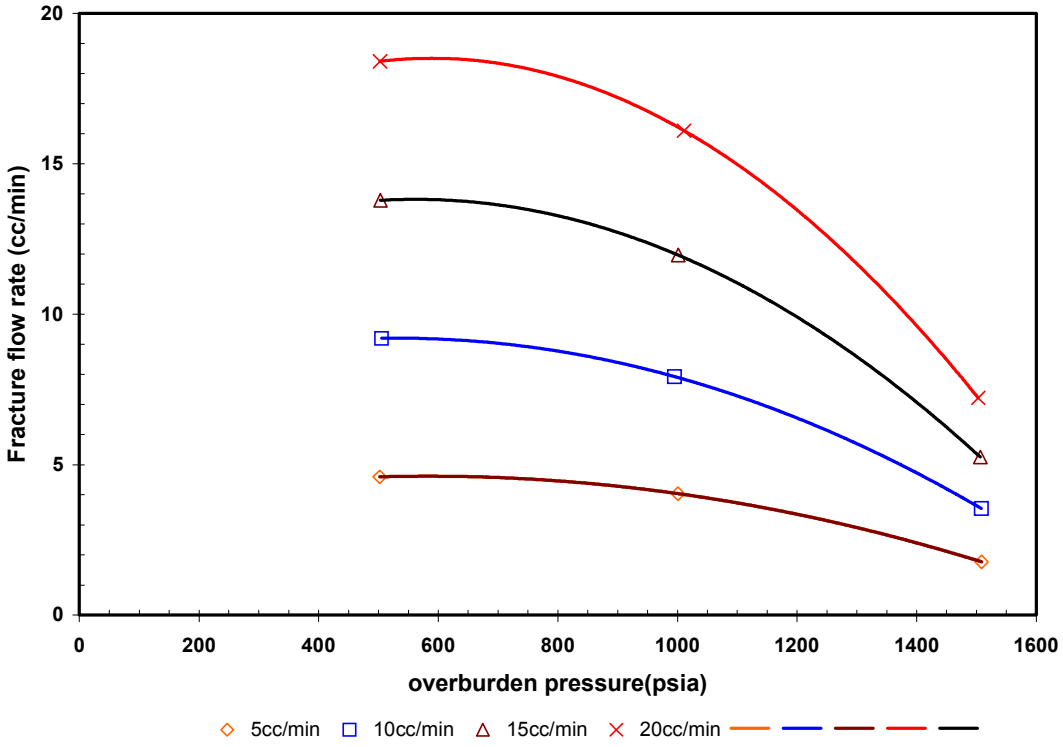

Fig. 1.6 – Effect of hydrostatic stress on fracture flow rate at different injection rate

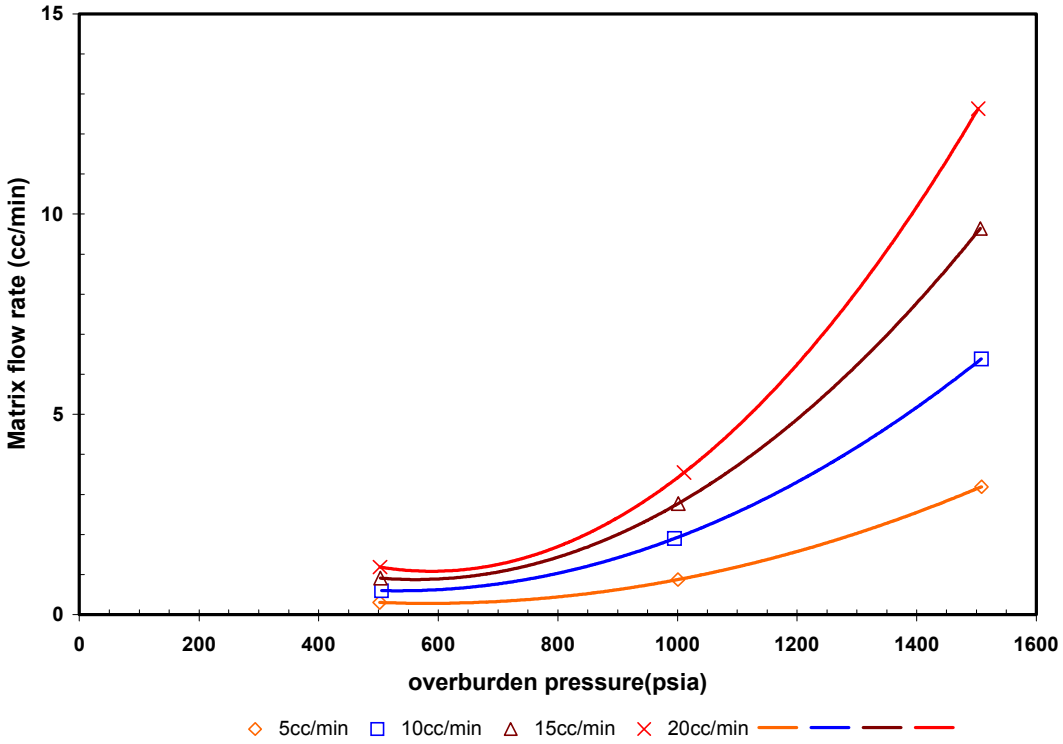

Fig. 1.7 – Effect of hydrostatic stress on matrix flow rate at different injection rate

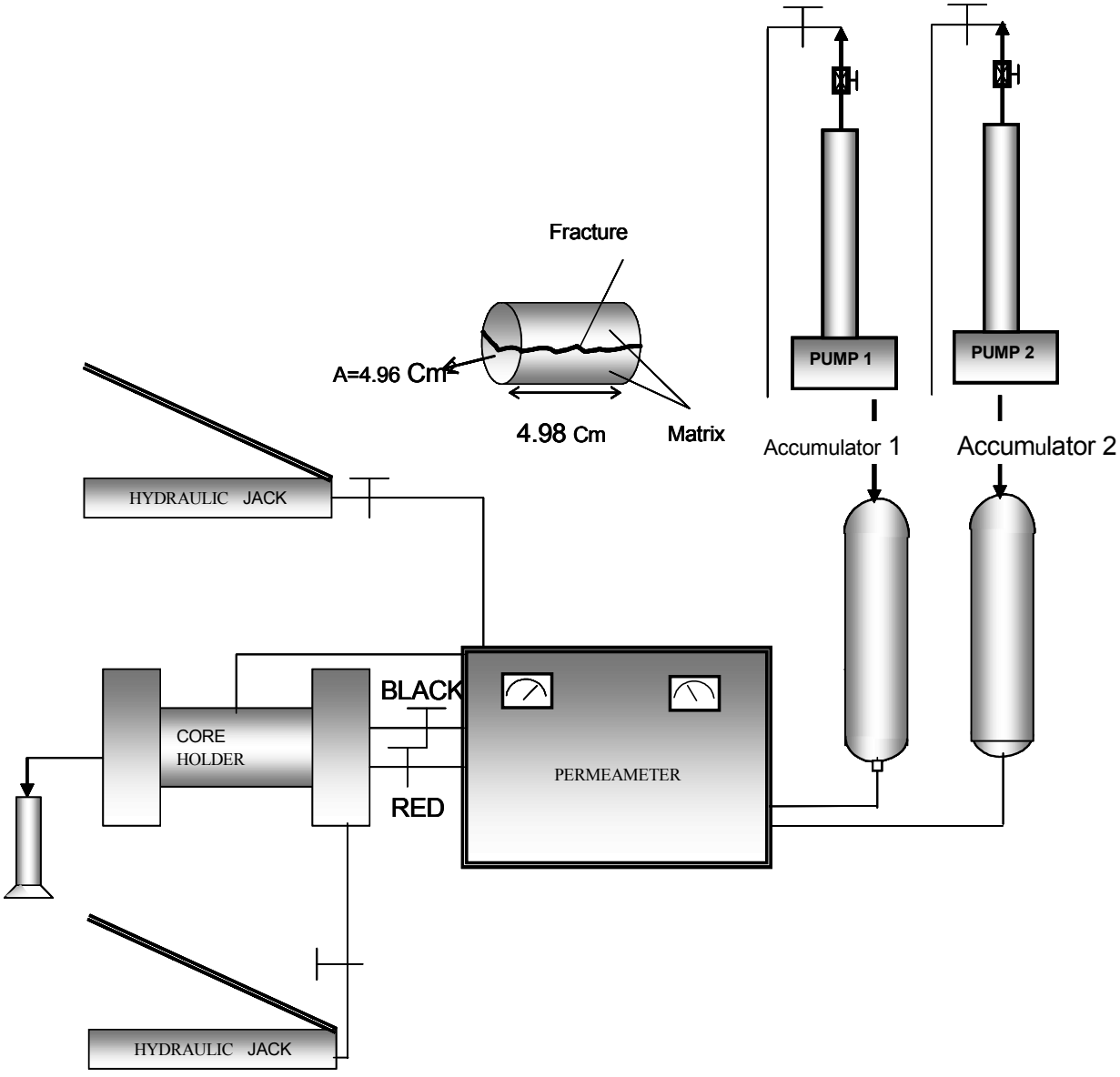

Fig. 1.8 - Triaxial stress experiment apparatus

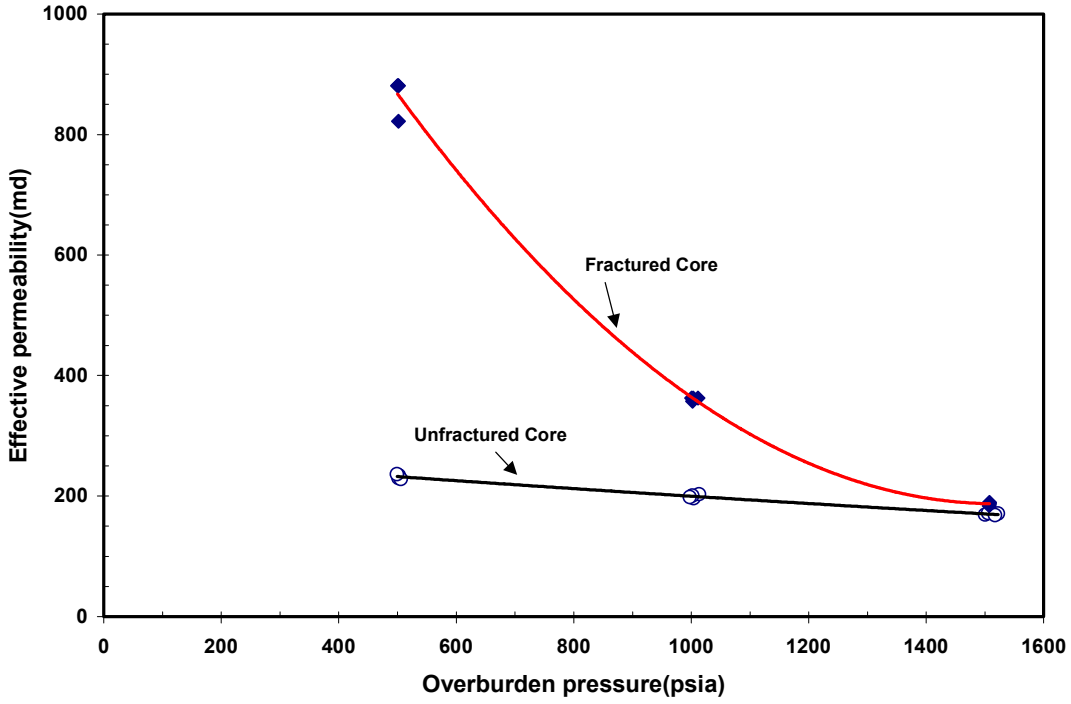

Fig. 1.9 – Permeability reduction due to triaxial stress

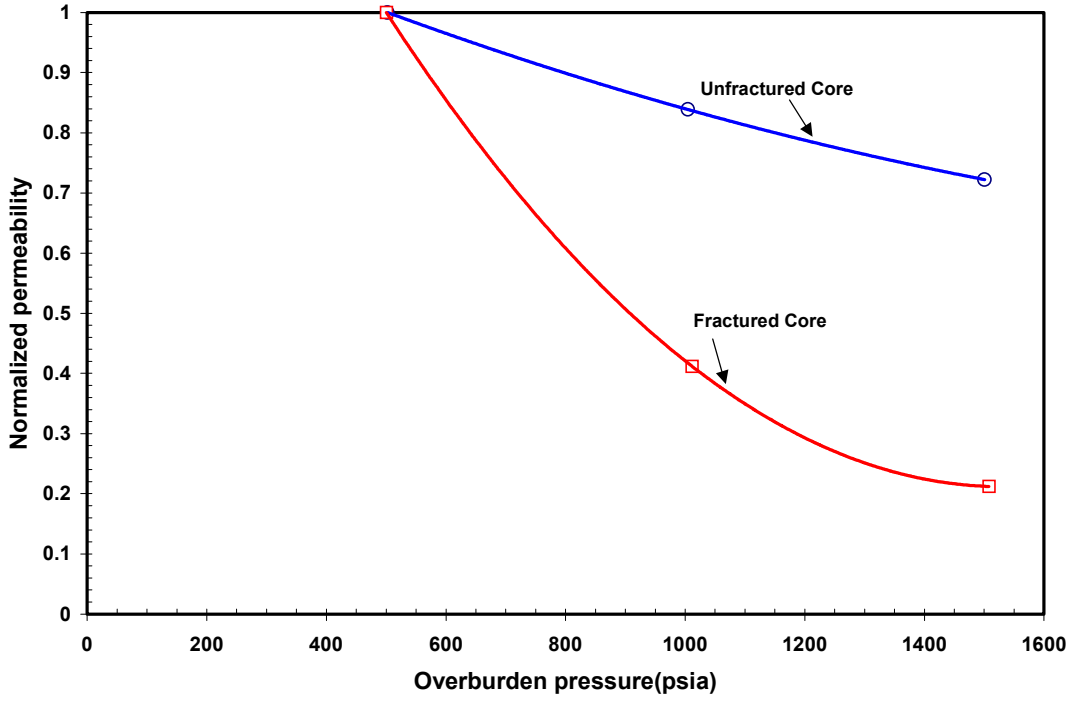

Fig. 1.10 – Normalization permeability reduction due to triaxial stress

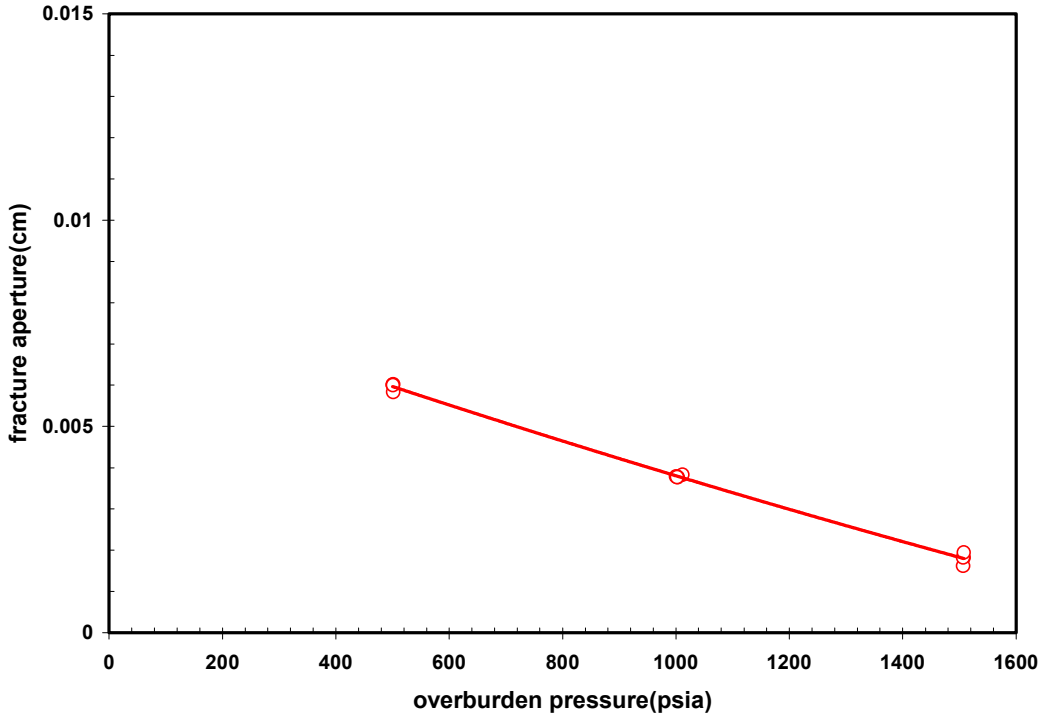

Fig. 1.11 – Fracture aperture reduction due to triaxial stress

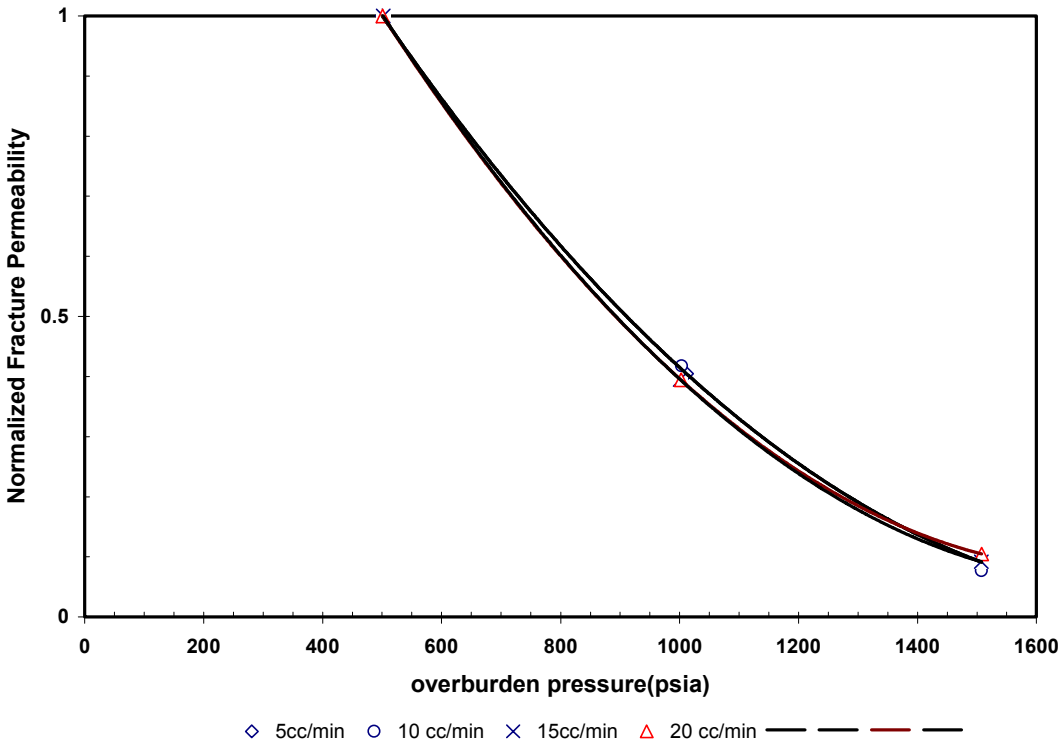

Fig. 1.12 – Normalized fracture permeability reduction due to triaxial stress

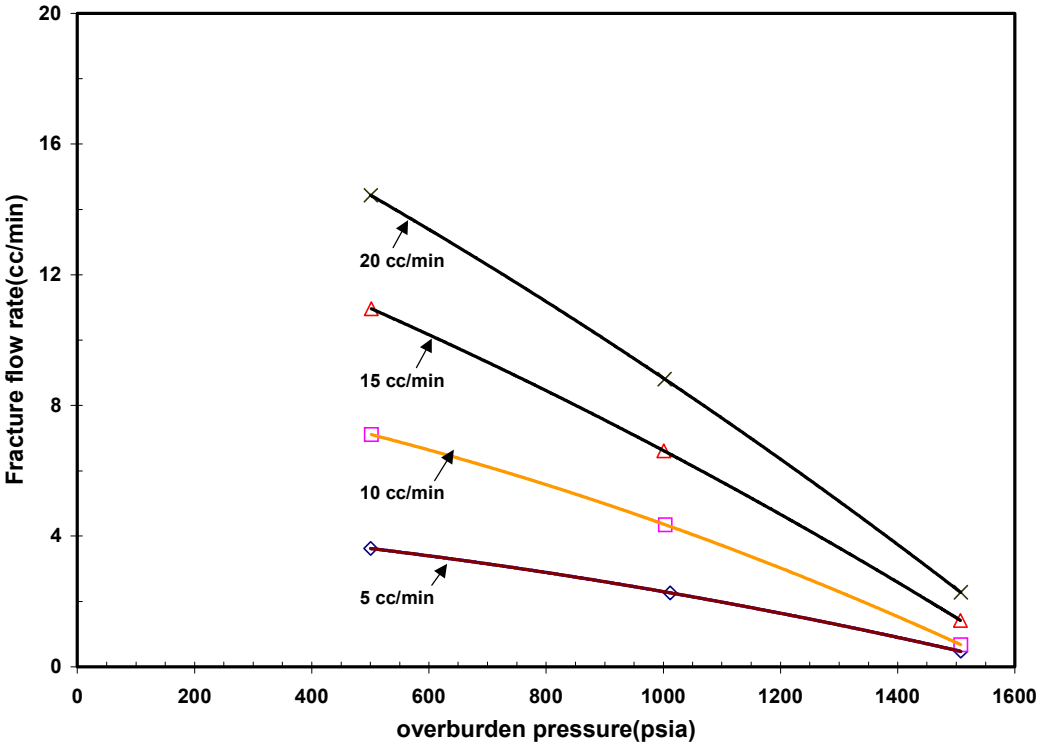

Fig. 1.13 – Effect of triaxial stress on fracture flow rate

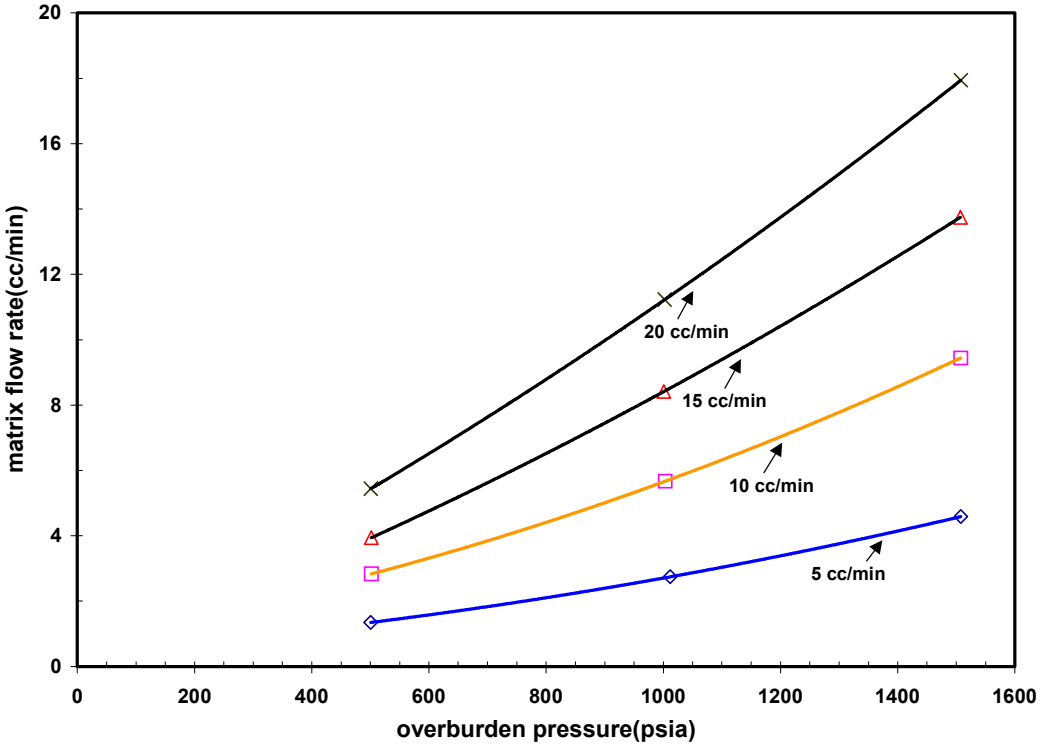

Fig. 1.14 – Effect of triaxial stress on matrix flow rate at different injection rates

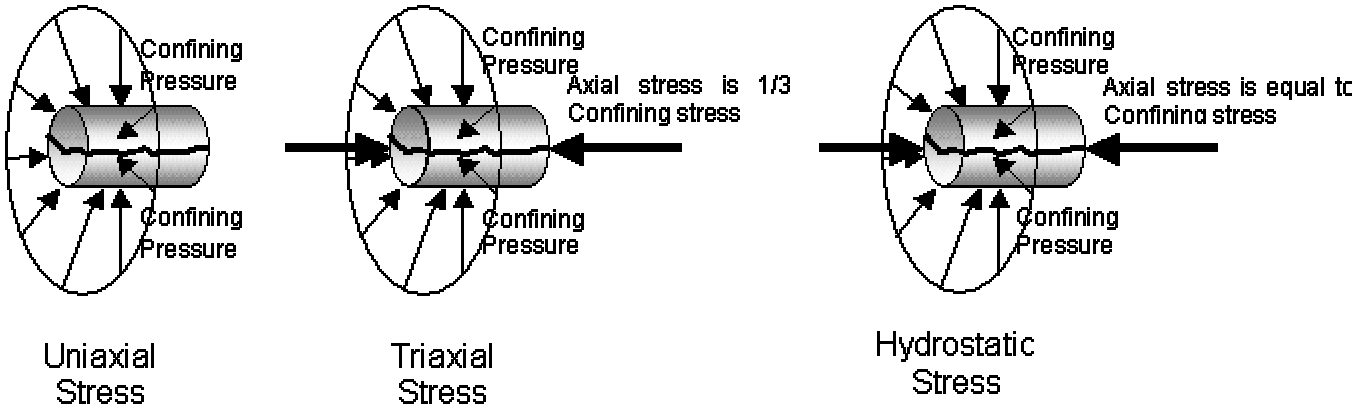

Fig. 1.15 - Illustration of uniaxial, triaxial and hydrostatic stresses

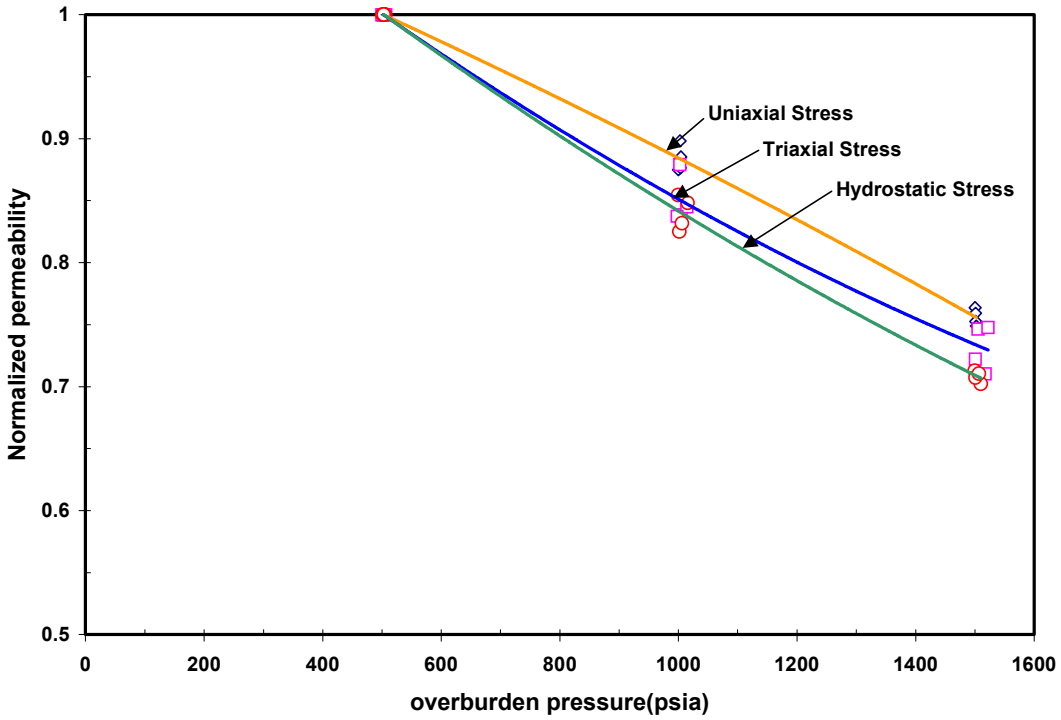

Fig. 1.16 – Comparison of matrix permeability reduction due to different applied stresses

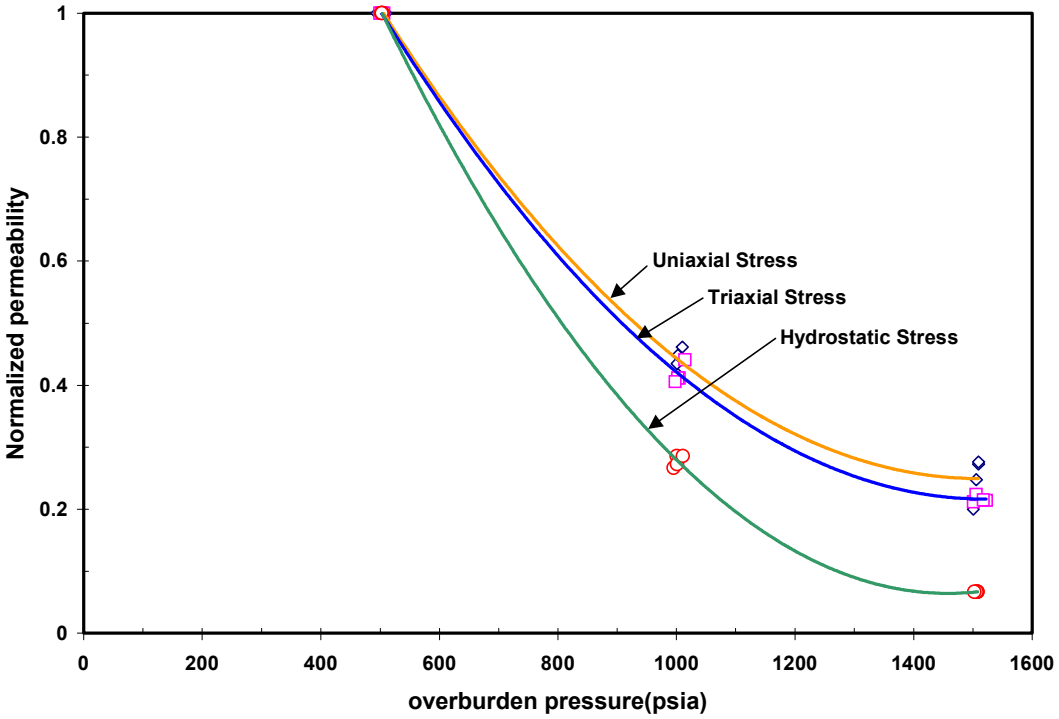

Fig. 1.17 – Comparison of effective permeability reduction due to different applied stresses

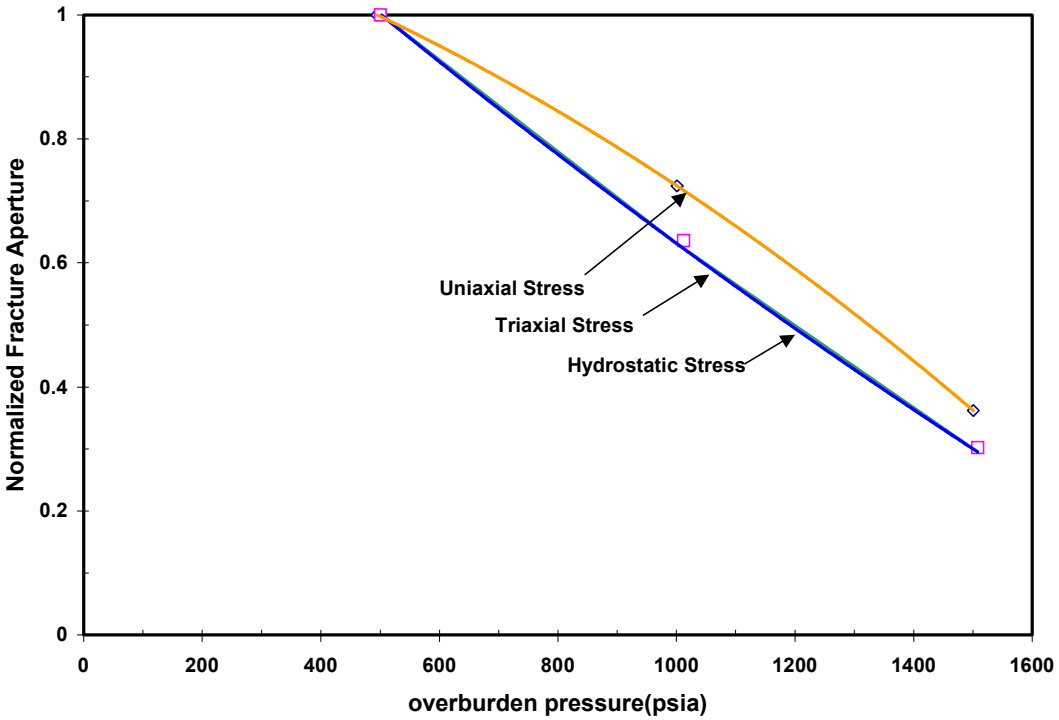

Fig. 1.18 – Comparison of fracture aperture reduction due to different applied stresses at injection rate of 5 cc/min

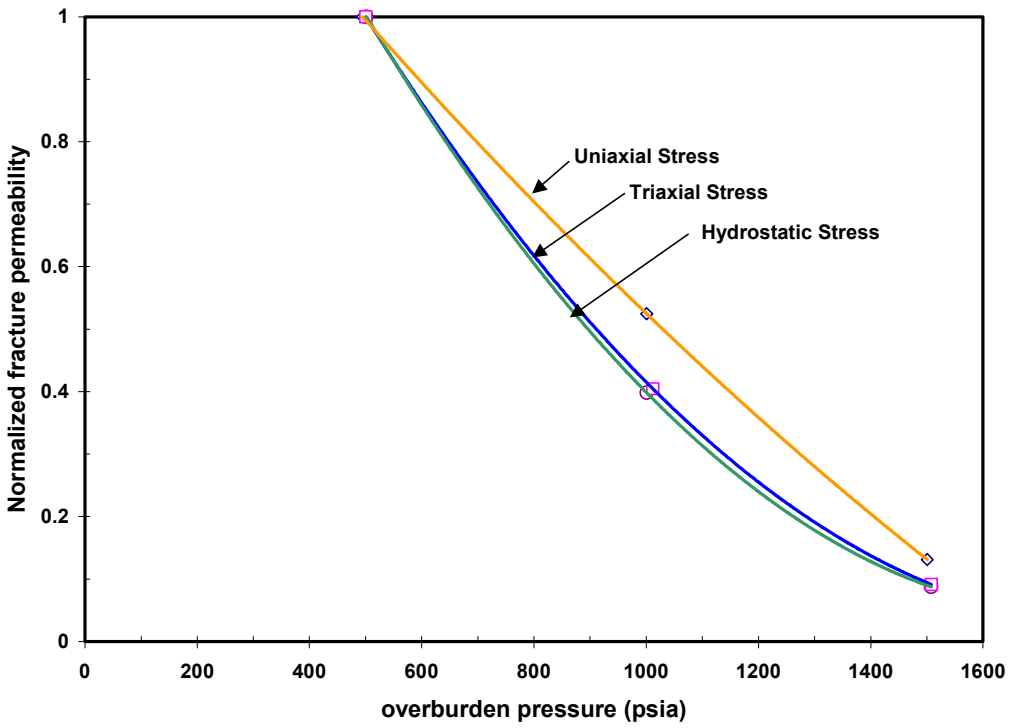

Fig. 1.19 – Comparison of fracture permeability reduction due to different applied stresses at injection rate of 5 cc/min

II. Preliminary Results of Imaging Imbibition Process Using X-Ray CT Scanner

2.1 Introduction

Imbibition is defined as the spontaneous absorption of a preferential wetting fluid into a porous medium with the simultaneous expulsion of the contained fluid. Imbibition is the most important mechanism of oil production in the waterflooding of fractured reservoirs. Counter current imbibition is the process in which water and oil flow through the same face in the opposite directions, whereas cocurrent imbibition is the process in which water and oil flow in the same directions. Often, there are existences of two interconnecting paths i.e. fractures and matrix in the reservoirs. The fractures constitute a continuous path for fluid flow in the reservoir, while the matrix blocks are discontinuous and provide the main storage for oil and gas.

The laboratory study includes static and dynamic imbibition experiments. Although the experiments are conducted at room temperature, the future work will be extended to the reservoir temperature. The main aim of the experiments is to obtain relative permeability analysis of both matrix and fractures and wettability of the core sample.

Wettability is described as the ability of a fluid to wet a solid surface in the presence of a second fluid. Amott (1959) defined wettability as the relative preference of a particular surface to be covered by one of the fluids under consideration. The displacement effectiveness and ultimate oil recovery by driving fluids such as water flooding depends on the wettability of the reservoir rock. After establishing the initial water saturation, the wettability index can be determined using the Amott test method. The determination of wettability index consists of two parts. The first part is spontaneous imbibition in water and the second part is followed by forced displacement by water.

Wettability index for water is determined by the following expression.

$$WI = \frac{V_{iw}}{V_{iw} + V_{dw}}$$

where WI is the wettability index, V_{iw} is the oil produced from the imbibition process and V_{dw} is the oil produced from the displacement process.

In the porous media, the wettability is generally classified as either homogenous or heterogeneous. For the homogeneous case, the entire surface has a uniform molecular affinity for either water or oil. But heterogeneous wettability indicates distinct surface regions that exhibit different affinities for oil or water. The homogeneous wettability is classified as strongly water-wet, strongly-oil wet and intermediate wet. The reservoirs are not always strongly water-wet, because some crude oil samples showed an ability to wet sand grains as explained by Bartell et al (1928). Later the terms intermediate-wet was discussed by Marsden et al (1962). The heterogeneous behavior of the rocks was discussed by Browns et al (1956). Mixed wettability refers to distinct and separate water-wet and oil-wet surfaces, which coexist in a porous medium. The mixed wettability study was conducted by Salathiel (1973). Speckled or spotted wettability refers to continuous water wet surface enclosing regions of discontinuous oil-wet surfaces or vice-versa. The speckled wettability was explained in detail by Morrow et al (1986).

The imbibition mechanism can be characterized by its rate and by the total amount of fluid displaced, which depends on the wettability. Most of the early experimental studies of imbibition were made with strongly water-wet system and constant fluid properties. Several investigators have introduced changes in fluid properties, rock properties and boundary conditions. Determination of the imbibition mechanism provides knowledge about capillary forces and displacement behavior that related to changes in the wetting behavior of the system. In laboratory, imbibition can be performed under two conditions, which are static and dynamic conditions.

Static imbibition is defined as the displacement of the non-wetting fluid by the wetting fluid through the action of capillary forces alone. Mattax *et al* (1962) studied the size of the rock sample for determination of imbibition rate. He also discussed rock characteristics such as porosity, permeability and the local variations of these parameters. Boundary conditions were analyzed by Iffly *et al* (1972).

Brownscombe *et al* (1952) introduced dynamic imbibition process. The process includes injecting on end of the single fracture and the water is produced on the other

end. The imbibition process occurs once the water is injected and the oil is produced. Graham *et al* (1960) presented the results of theoretical and experimental studies of dynamic water injection. They found that the imbibition is rate sensitive and proportional to the square root of the matrix permeability, interfacial tension, contact angle and viscosity ratio.

The main aim of this study is to prepare the static and imbibition experiments for the imaging saturation profiles using X-Ray CT scanner.

2.2 Experimental Description

Berea core samples are used for the static and dynamic imbibition experiments (Table 2.1). Berea sandstones were used because it is widely used as a standard porous rock for experimental work in the petroleum industry. Refined oil is used for the experiments.

2.2.1 Brine composition

Synthetic brine was used in the experiments. It was prepared by dissolving Nacl and $CaCl_2.2H_2O$ in distilled water. The brine compositions are shown in Table 2.2.

2.3 Experimental Procedure

2.3.1 Core Saturation

Dry core samples were weighed on a balance. The core sample was then saturated with deaerated brine using a vacuum pump for at least 12 hours. After saturating the core samples with brine, a period of 3 days was allowed for the brine to achieve ionic equilibrium with the rock.

2.3.2 Core Flooding

The saturated core is inserted in the Hassler-Type core holder. Overburden pressure is applied in the radial direction. An initial overburden pressure of 500 psi is applied. This is followed by core flooding with the brine solution at flow rates of 5, 10, 15 and 20cc/min. The pressure drop across the core is recorded in the transducer. The

experiments are repeated for overburden pressures of 1000 psi and 1500 psi and the corresponding pressure drops are recorded. Subsequently, the core is flooded with oil to displace the brine. The core flooding is done till the irreducible brine saturation is achieved. This may take many hours of flooding.

2.3.3 Imbibition Cell

The core is then taken out of the core holder and introduced in the imbibition cell. The imbibition cell is filled with brine solution and the imbibition process is called the counter current imbibition. The apparatus is a simple glass container equipped with a graduated glass cap. The outlet valve is connected to the vacuum pump to remove any air trapped during the transfer of the core. The recovery of oil initially is noted every half an hour. Later the reading was taken once after 24 hours. The imbibition takes about 21 days. Figure 2.1 shows the imbibition cell that is used for the experiment.

2.3.4 Wettability Index Determination

To determine the wettability index for water (I_w), the core is transferred to Hassler sleeve after the spontaneous imbibition for brine displacement. The injections were performed at room temperature.

2.4 Experimental Results

2.4.1 Effect of Overburden Pressure on Absolute Permeability

Absolute Permeability of the rock decreases with the increase in the applied stress. Figure 2.2 shows the effect of overburden pressure on permeability of the core sample. The permeability of the core affects the imbibition process. If the permeability of the rock is high, then the imbibition is faster and the recovery of oil is high.

2.4.2 Brine Recovery as a function of time

When oil is injected in the core, brine is displaced from the core. The recovery of brine depends on the drainage capillary pressure. Once the saturation of water decreases, the capillary pressure increases in the rock. Oil flooding can be done until the core

reaches irreducible water saturation. Then any further injection of oil will result in almost 100% oil cut. Figure 2.3 shows the plot between brine recoveries and time. The production of brine is much less after about 5 hours of oil injection at a flowrate of 1 cc/min. Figure 2.4 displays the result in terms of percentage of initial water saturation. The initial water saturation decreases and after some time it stabilizes. This is the point of irreducible water saturation. The capillary pressure will be high.

2.4.3 Oil Recovery as a function of time

When the imbibition process starts, the brine imbibes in the core and extracts oil out of the core. Once the imbibition starts, the water saturation increases and the oil saturation decreases until irreducible oil saturation is achieved. It may take several days to attain irreducible oil saturation. The imbibition process is faster initially and then stabilizes after some time. If the core is strongly water-wet then the recovery will be greater. Also the imbibition process is fast. If the initial water saturation is more at the start of the imbibition process then the imbibition occurs at a faster rate. This is because the mobility of the water is high due to the initial water saturation. However the capillary pressure will be low due to the initial water saturation. Hence the final amount of oil recovered will be less and the percentage of initial oil in place is less compared to the condition with low initial water saturation. Figure 2.5 shows the plot between oil recoveries as percentage of IOIP against time. The recovery of oil is very less after about 10 hours of imbibition.

2.5 References

1. Amott, E.: “Observations Relating to the Wettability of Porous Rock”, *Trans*., AIME, 216, 1959, 156-162.
2. Bartell, F. E. and Miller, F. L.: “Degree of Wetting Silica by Crude Petroleum Oils”, Ind. Eng. Chem., July 1928, 20, N0.7, 738-742.
3. Marsden, S. S. and Nikia, P. A.: “The Wettability of the Bradford Sand I.”, Producers Monthly (May 1962), 2-5.

4. Salathiel, R. A.: “Oil Recovery by Surface Film Drainage in Mixed Wettability Rocks”, J. Pet. Tech. (Oct 1973), 1216-1224.
5. Morrow, N. R., Lim, H. T. and Ward, J. S.: “Effect of Crude Oil Induced Wettability Changes on Oil Recovery”, SPEFE (Feb. 1986), 89-103.
6. Mattax., C. C. and Kyte, J. R.: “Imbibition Oil Recovery from Fractured, Water Drive Reservoir”, Soc. Petr. Eng. J. (June 1962), 177-84.
7. Iffly, R., Rousselet, D. C. and Vermeulen, J. L.: “Fundamental Study of Imbibition Process in Fissured Oil Field”, paper SPE 4102 presented at the 1972 Annual Fall meeting of SPE, San Antonio, Texas.
8. Brownscombe, E. R. and Dyes, A. B.: “Water Imbibition Displacement: A Possibility for the Spraberry”, Drill. And Prod. Prac., API (1952), 383-390.
9. Hassler, G. L.: U. S. Patent No. 2.345,935 (1944).
10. Petroleum Engineering Handbook, Chapter 28: “Relative Permeability”.
11. Schechter *et al*: “Advanced Reservoir Characterization and Evaluation of CO2 Gravity Drainage in the Naturally Fractured Spraberry Trend Area,” Final Technical Report, DOE contract No.: DE-FC22-95BC14942 (June 2002).

Table 2.1 - Core sample used in the experiment

Diameter	3.602 cm
Length	4.684 cm
Area	10.190 cm^2
Bulk volume	47.727 cc
Pore Volume	11.514 cc
Porosity	24.12 %

Table 2.2 - Synthetic Brine Composition

Salts Content	Concentrations (mg/L)
Nacl	122,699
$CaCl_2.2H_2O$	7,497
Total Dissolved Solids	130,196

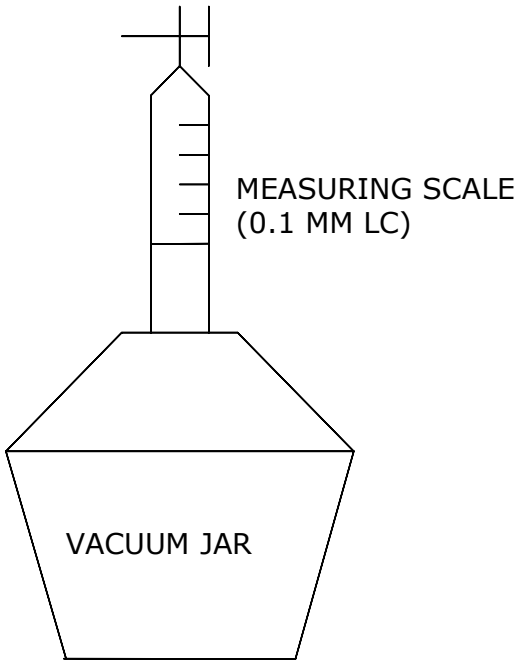

Fig. 2.1 – Static imbibition apparatus

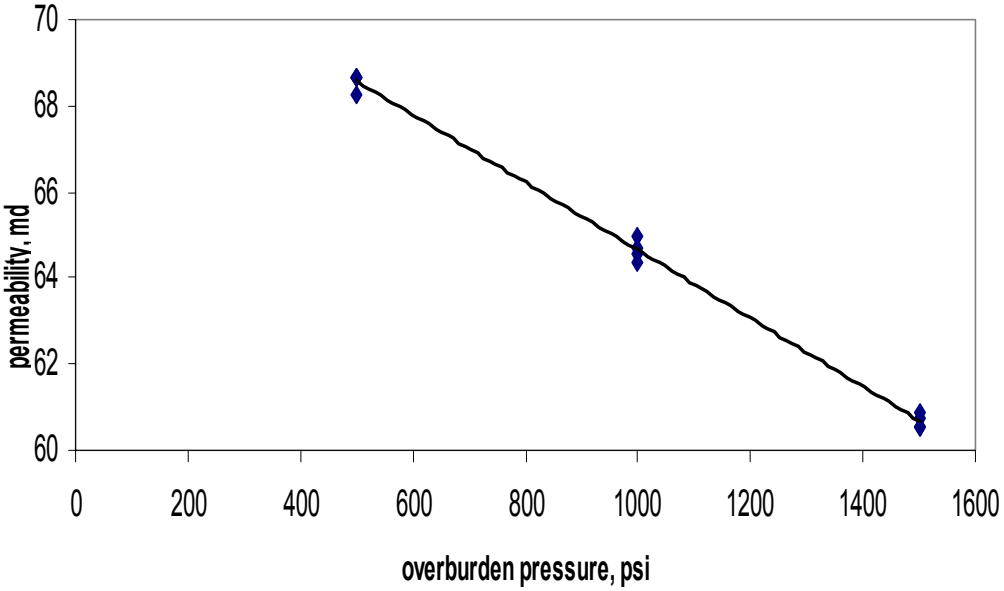

Fig. 2.2 – Reduction of absolute permeability due to an increase in overburden pressure

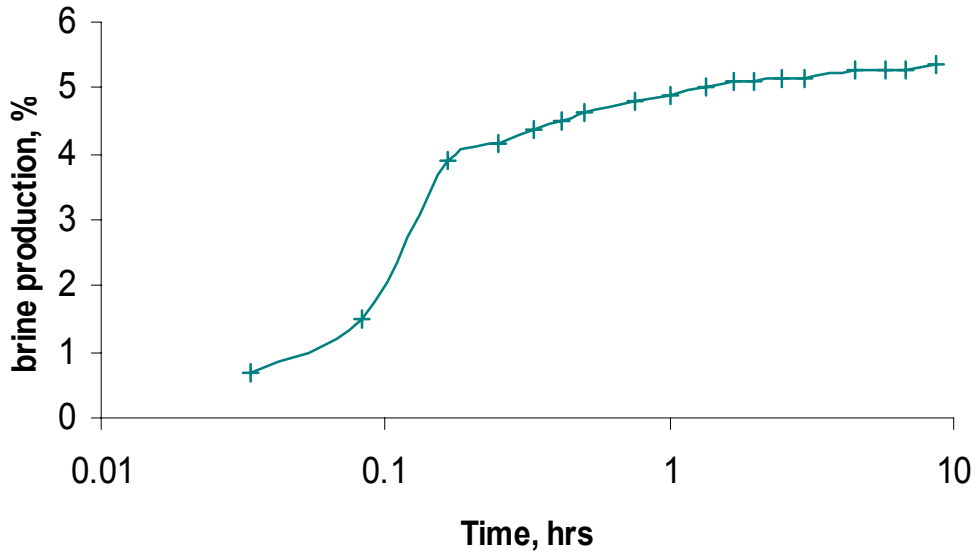

Fig. 2.3 – Brine recovery over imbibition time

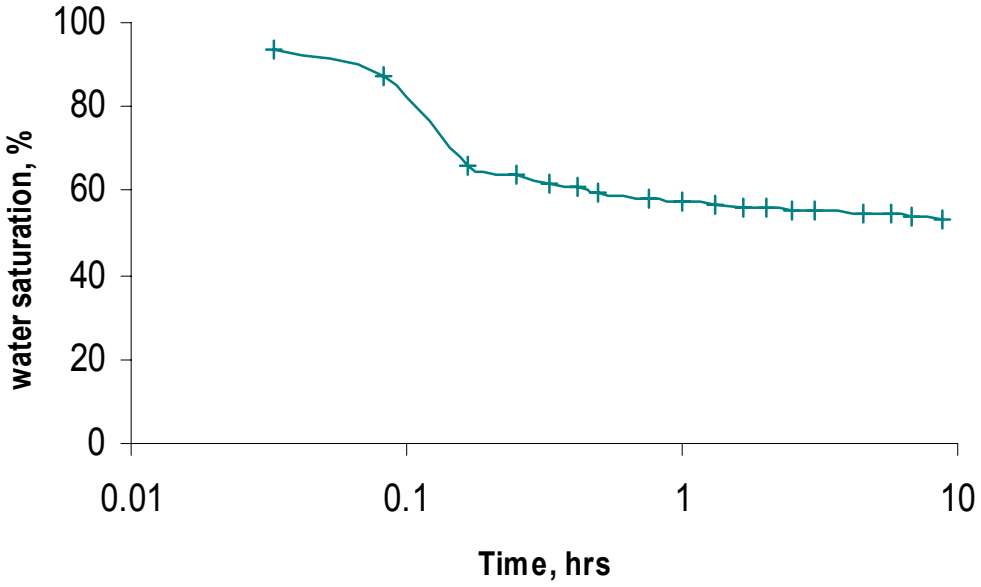

Fig. 2.4 – Water saturation profile over imbibition time

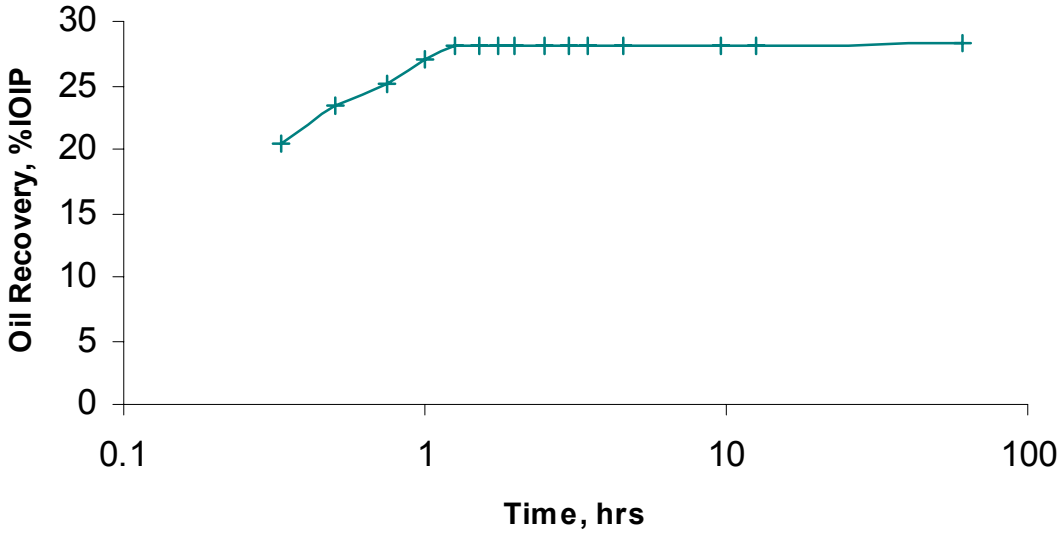

Fig. 2.5 – Oil recovery over imbibition time

III. Modeling Fluid Flow Through Single Fracture using Experimental, Stochastic and Simulation Approaches

3.1 Introduction

The search for hydrocarbons has been expanded into harder-to-evaluate formations, where highly potential and profitable hydrocarbon reserves are located. Over the past few years, extensive studies have been conducted on fractured reservoirs, because they are difficult to simulate due to the complexity of fractured reservoirs and also the presence of tectonic discontinuities.

The production capabilities have been restricted because of the lack of knowledge about fractures and flow, which occurs through fractures. Understanding the fluid flow characteristics of fractures is very important to modeling flow through fractures and hence extend it to the behavior of the reservoir. Fracture aperture and connectivity are the most critical properties controlling flow and contaminant transport in the saturated zone. This is because under laminar flow the transmissivity of a planar smooth-sided fracture is very sensitive to aperture size. Transmissivity seems to be proportional to the cube of the aperture. This is known as the "cubic law" of fracture flow.

Fracture permeability is usually estimated by a cubic law that is based on the theory of hydrodynamics for the laminar flow between flat plates. However, the cubic law is too simple to estimate the fracture permeability correctly, because the surface of real fracture is much more complicated and rougher than the surface of a flat plate. Several researchers have shown that the flow characteristics of an actual fracture surface would be quite different due to the effect of tortuosity, impact of surface roughness and contact areas. But the general conclusion from these efforts is that the cubic law is valid when an appropriate average aperture can be defined. Many average apertures have been proposed, and for some cases, some work better than others. Nonetheless, to date, these efforts have not converged to form a unified definition on the fracture aperture needed in the cubic law.

In this study, therefore, we show that the cubic law could still be used to model small-scale and field-scale data as long as it is modeled effectively, accounting for the effect of surface roughness associated with the fracture surface. We understand the surface roughness has a major part to play in modeling flow though fractures. The notion of a perfectly smooth parallel plate theory is no longer assumed in this research because it does not represent the true picture of a fracture surface.

We performed laboratory experiments to support our study and attempted to match the observed results by modifying cubic law to account for the friction associated with the flow through fractures. Though several papers have discussed the effect of friction in flow considerations, the application of the friction factor into simulations has not been looked into with reference to the experimental results. This stimulates the current effort to develop a general model for simulating flow through fractures by incorporating the friction factor or the flow modification factor to alter the fracture permeability distribution on the surface of the fracture. The goal of this research is to examine the effect of surface roughness for flow through fractures and to effectively incorporate them into simulations with the aid of geostatistics. Since research has been supported with experimental results, the consistency of the results enabled us to define a methodology for single fracture simulation.

3.2 Previous Research Efforts

Early investigators based their idea that a parallel plate concept would be utilized to understand the concept of fluid flow through fractures. The first comprehensive work on flow through open fractures was by Lomize (1951). He used parallel glass plates and demonstrated the validity of the cubic law as long as the flow was laminar. He also investigated the effects of changing the fracture walls from smooth to rough and, finally, to a model with different fracture shapes. He introduced the concept of defining the surface roughness based on empirical data. Later he developed a flow regime chart that takes into account the effects of roughness and turbulent flow in open fractures. He proposed to include the roughness factor into the flow equation. Loius (1969),

independently performed similar experiments and reached essentially the same conclusions.

It was Snow (1969) who used this concept to simulate real fractures. The cubic law governs the viscous flow through a fracture with smooth and parallel walls. He discussed the need for careful assessment since real joints in a rock do not represent the parallel plate model assumed then. With this idealization he treated flow along intersecting fractures as being proportional to the cubic of the apertures and to the projection of the field gradient generally not parallel to neither of the two fractures.

Sharp (1970) proposed an empirical flow law for natural fractures that was based on the "effective" aperture, which is the difference in the opening from the initial condition, and the net flow rate obtained from a calculation of measured flow rate minus that observed under the initial closed condition.

Iwai (1976) conducted a comprehensive study of fluid flow through a single fracture and investigated the validity of the cubic law of fluid flow through a single natural fracture. One of the important features of his experiments was that the fracture planes had contact area as well as roughness. Utilizing this observation an idealized fracture model can be constructed in which flow paths are represented by an opening which varies continuously normal to the flow, but with constant aperture in the flow direction. The aperture variation normal to the flow direction is represented by the aperture distribution in the fracture.

Nuezil and Tracy (1980) modeled a fracture flow, by representing fractures as a set of parallel openings with different apertures. They generated an aperture distribution through a lognormal distribution and studied the flow through numerical analysis. They showed that the flow conformed to the cubic law and also that the maximum flow occurs through the highest apertures, thereby quoting that the flow takes a preferred path. Thus in their analysis, the flow depended on the tail of the frequency distribution. They stated that the flow not only depends on the aperture but also the distribution parameters; the first and the second moment of distribution in their case.

Witherspoon et al. (1980) stated that cubic law was found to valid whether the fracture surfaces were held open or were being closed under stress, and the results were independent of rock type. Permeability was uniquely defined by fracture aperture and was independent of the stress history. The effects of deviations from the ideal parallel plate concept only caused an apparent reduction in flow and may be incorporated into the cubic law by a flow modification factor.

Tsang and Witherspoon (1983) studied the dependence of mechanical and fluid flow properties of a fracture on its roughness and sample size. They correlated the shape of the aperture distribution to the specific fractures of the stress-strain behavior and also to the fluid flow characteristics. They concluded that the roughness of a fracture wall could be characterized by a large-scale undulation. Also it is the large-scale undulation that determines the shape of the aperture distribution curve. They also stated that if the fracture surfaces were not well matched, it could lead to a larger mean and variance. Theoretical and experimental studies of fracture geometry have shown that the parallel plate model does not accurately depict a rock fracture. For example, Tsang and Witherspoon (1983) present figures of actual fracture profiles derived from Bandis et al. These fracture profiles are non-parallel and consist of both a large-scale undulation and small-scale roughness.

Tsang (1984) investigated the effect of tortuosity in fluid flow through fractures and found that it plays a significant role. He represented the flow paths with electrical resistors placed in a 2 dimensional grid. Fracture apertures obtained from both laboratory and from hypothetical analytic function were used in the study. He found out that, the more small apertures that are present in the aperture distribution, the more the effect of tortuosity. He related the increase in tortuosity and the decrease in connectivity of the fluid flow paths to the increase in fracture contact area. Though he did not model the effect of surface roughness in his study, he stated that the tortuosity along with the effect of surface roughness depresses the flow rate from the value predicted by the parallel plate theory by three or more orders of magnitude.

Brown (1987) investigated the effect of surface roughness on fluid flow through rock joints. He observed that the deviations of fluid flow from the cubic law could merely stem from the fact that the surfaces are rough and contact each other at discrete points. He performed a simulation of flow between rough surfaces using a fractal model of surface topography. The solution was the local volume flow rate through the rock joint. He solved this flow rate to derive the "hydraulic aperture" using the cubic law. He concluded that for small aperture separation the topography did have a significant effect through tortuosity, as stated by many researchers. And also he found out that the parameter most affecting the fluid flow through rock joints is the ratio of the mean separation between the surfaces to the root mean square surface height. This parameter describes the nature of the roughness that protrudes into the fluid and accounts for most of the disagreement with the parallel plate model.

Tsang and Tsang (1987) developed a conceptual model to effectively model flow channels for fractured media. They employed a log normal distribution and generated a statistical aperture distribution based on the mean, variance and spatial correlation length. They made predictions for tracer breakthrough curves in the case of a single fracture with varying overburden stress based on their conceptual model, which seem to correspond well with the one provided by Moreno et al (1988). They also expressed the importance of laboratory experiments to validate their model.

Other studies indicate that the fracture aperture may vary either as a correlated random variable (Moreno et al., 1988) or as a random variable described through a fractal model (Brown, 1987). Work by other researchers, such as Neuzil and Tracy (1981), Brown (1987), Tsang and Tsang (1987), Tsang et al. (1988) and Moreno et al. (1988), have shown that the flow through a fracture follows preferred paths or flow channels due to the variation in fracture aperture. One aspect on which everybody agrees is that the fractures are not parallel walls but are themselves 2-dimensional networks of variable aperture. Hence, fluid flow in single fractures probably does not strictly follow the cubic law.

The focus of much research is to understand and quantify these deviations from the cubic law. Also these investigations were associated with open fractures, and, of course, one

will encounter many situations in the field where the fractures are not open. Usually, fracture surfaces have some degree of contact, and the effective aperture will depend upon the normal stresses acting across the discontinuity. But since a part of the flow is blocked by asperities, there were concerns whether the cubic law would actually be valid. Several researchers have proposed a new model wherein the fracture is represented by a set of parallel plate openings with different apertures. The model leads to a modified Poiseuille equation for flow, which includes an aperture frequency distribution for the fracture.

In the last two decades, researchers have employed a more realistic description of a rock joint with a range of apertures, and the impact of the aperture variation with a single rock joint on its flow properties has been recognized (Tsang and Witherspoon, 1981, Tsang 1984, Brown 1987). The techniques used in the industry to obtain aperture measurements include : 1) joint surface profiling 2) low melting point metal injection 3) resin casting technique. These measurements have provided useful and important data for the basic studies of flow and transport through variable-aperture fractures. However, in practical field problems it is neither feasible nor practical to make such detailed measurements of apertures in all fractures participating in the flow and transport. Furthermore aperture measurements of exposed fractures at the borehole walls, tunnel walls of core samples may be affected by the drilling or evacuation process so that they may not be representative of the fractures in the rock mass.

Tsang and Tsang (1990) chose a statistical description of a fracture with variable apertures by means of three parameters, two related to the aperture distribution: mean aperture and the standard deviation, and one to the spatial arrangement of the aperture, the spatial correlation length. This was similar to their previous study done (1989) where they generated fracture aperture distribution by the same means and through simulation study they concluded that the majority of the flow tends to be concentrated in certain preferred paths. They performed numerical flow and transport experiments with them with particular emphasis of correlating the fracture geometry parameters with observed measurable hydrological quantities. Though they advocated the need for this kind of

hydrological measurements and interpretation they concluded that the correspondence between observations and the hydrological properties is still ambiguous.

Although several researchers have analyzed the fracture flow and its deviations from the cubic law in great detail, none of them provide a definite picture of modeling both rough surfaces and the roughness factor associated with it. Many conceptual models developed in the past have not been corroborated through effective laboratory results. In our research we performed experiments with a fractured core to study the flow behavior in fractures with increasing overburden pressures. We then analyzed the laboratory measurements and derived the average fracture aperture width using the cubic law. The focus of our research is to prove that accurate results could be obtained from the cubic law if modified to account for the effect of roughness.

We generated a two dimensional network of fracture aperture distribution using stochastic analysis (lognormal distribution), following similar approaches by earlier researchers. We then accounted for the effect of surface roughness by means of a friction factor to obtain a modified permeability distribution in a fracture and used a commercial simulator to simulate the experiments. We have proved from our modeling that a single fracture of constant aperture fails to model the experimental results and hence the cubic law. Since we had the comfort of experimental results to support our model, we have an effective methodology to simulate single fracture with fracture aperture distribution.

3.3 Distribution of fracture apertures

3.3.1 Aperture measurements

Fracture aperture is the key parameter in determining the flow and transport characteristics of fractured media. In natural fractures there is usually a large distribution of fracture apertures even within a single fracture. The fracture aperture distribution is controlled by a number of factors. The history of mechanical, thermal and chemical stresses on the material, from before it fractured, through the primary fracturing process and the subsequent fracturing episodes on to its current state impact significantly the

nature of the fracture aperture distribution. A sudden release of the confining pressure may result in a widening of the fractures. Fracture spacing, which may be a result of both material strength and stress history, also affects the fracture aperture distribution. (van-Golf-Racht, 1982)

Prediction of the fracture aperture distribution given the material properties and stress history is next to impossible, since the material is likely to fail at flaws or inclusions in the matrix, which cannot be captured in the averaged material properties. Field determination of the fracture aperture distribution, or even simply mean aperture, is currently an area of active research. Several direct techniques for detecting and imaging fractures are under development.

Kumar et al (1997) employed nuclear magnetic resonance imaging techniques to measure the spatial distribution of apertures. They found that they were in good agreement with the normal and hydraulic aperture values from cores. Detwiler et al (1998) measured the fracture aperture filed using a transmitted light. They showed how the error in aperture field measurement could influence the results of flow and transport simulations. Lerner and Steele (1998) developed a new field technique where a NAPL (Non-Aqueous Phase Liquid) is injected into a fractured sandstone aquifer and the transient pressure response from it was used to derive an aperture profile by reverse numerical modeling of the field data. But they were only able to measure fracture apertures > 40 um.

Indirect techniques of measuring the statistics of the fracture aperture distribution (arithmetic mean, geometric mean and standard deviation) include pumping and tracer injection tests. These are currently the most accurate means of assessing fracture aperture and its distribution in the field. At the laboratory scale, a much higher resolution can be attained in the determination of the fracture aperture distribution. The higher resolution can be used to increase our understanding of the controlling mechanisms and key parameters for flow and transport in fractured porous media.

Several techniques have been applied to determine fracture aperture in the laboratory. The two surfaces of an open fracture can be scanned using a surface profiler (Brown et al., 1986), providing a map of the surface roughness at a theoretical resolution of 10 μm for surface features. The two halves are then closed using a precise guidance mechanism.

The fracture aperture distribution is now measured by knowing the distance between the two halves. Although the principle of this technique is very precise, there is a high probability that the confining pressure may change during a flow experiment, or that the referencing between the two halves may not be adequate, resulting in an error in the estimated fracture aperture distribution. In addition, the surface profiling process may affect the surface due to the direct application of mechanical force.

The fracture aperture distribution can also be determined by the resin casting technique and low melting point metal injection. These methods may yield the desired aperture information, but render the fracture useless for flow experiments. Non-intrusive methods of determining the in-situ fracture aperture, within a core holder, at a given confining pressure, are thus more desirable. This would call for the use of computer-aided Tomography or X-Ray CT scan. This would lead to very high processing costs, which only a few companies could afford. Therefore alternative methods for finding fracture aperture width and the fracture distribution have to be sought.

As an alternative to deterministic models, some investigators have used stochastic methods of characterizing fracture occurrence and flow in fractures. In the past several researchers have used geostatistics to generate the fracture aperture map, using parameters like mean fracture aperture, variance of the distribution and spatial correlation length. This process is effective and does not involve huge monetary resources and its usefulness in modeling purposes is unparalleled. Though it may not be a true representative of the fracture aperture system, they play an important role in characterizing a fracture system.

3.3.2 Fracture Aperture Definition

Brown (1987) states that the "definition of the 'aperture' of a rough-walled fracture is not unique." Due to the physical nature of rock fractures, researchers have used different definitions of the fracture aperture in the literature. The rough surfaces of a fracture are often depicted as distributions of apertures. Much research has focused on the mean, or arithmetic average, aperture of this distribution, and its relation to fluid flow in the fracture (Neuzil and Tracy, 1981; Brown, 1987; Tsang et al., 1988).

Brown used several aperture-averaging formulas, including arithmetic average aperture, in the cubic law to approximate the fluid flow in his numerically simulated fractures with isotropic random aperture fields. He determined that the flow calculated from the cubic law using the arithmetic average aperture, instead of the other aperture averaging formulas, better approximated the flow from his numerical simulations.

Flow characteristics are strongly controlled by fracture apertures. In order to understand the fracture aperture system, it is necessary to study the difference between mechanical and hydraulic apertures. Reneshaw (1995) investigated the relationship between mechanical and hydraulic apertures. He defined that the arithmetic mean of the fracture apertures, expressing the average distance between the fracture walls, as mechanical aperture. As stated earlier aperture derived from the cubic law is referred normally as the hydraulic aperture. He concluded that the cubic law can predict the fluid flow through fractures as long as an appropriate average fracture aperture is used.

A number of researchers have shown that the aperture values of laboratory core samples usually follow a skewed distribution well approximated by a lognormal distribution. In this research we have used geostatistical methods to generate a fracture aperture system through a lognormal distribution and then perform flow experiments through them and attempt to match the experimental results. Though this method is exhaustive, it has proved to be effective. Basic concepts of lognormal distribution are discussed in subsequent paragraphs below.

3.3.3 Log – Normal Distribution

Log normal distribution is closely related to the normal distribution. If the logarithm of a variable is normally distributed, then the variable itself is log normally distributed. The lognormal distribution is skewed with a long tail on the right hand side. However, after transforming the data by taking the log of the variable, the distribution becomes symmetric and normal.

If we consider X to be a log normally distributed variable, then we can define Y= ln X, where Y is the value of the natural logarithm of the random variable X. if the mean of the

variable Y is α and the variance is β^2, we can write the probability density function for the variable X as ,

$$f(x) = \frac{1}{x\beta\sqrt{2\Pi}} \exp\left[-\frac{1}{2}\left(\frac{\ln x - \alpha}{\beta} \right)^2 \right] \tag{1}$$

It can be shown that the mean and variance of the random variable X, is related to the mean and variance of the transformed variable Y. we can write,

$$\beta^2 = \ln\left[1 + \frac{\sigma^2}{\mu^2} \right] \tag{2}$$

and also,

$$\alpha = \ln \mu - \frac{\beta^2}{2} \tag{3}$$

where μ is the mean of the variable X, and σ^2 is the variance of the variable X. so given any standard mean and variance of a variable , we can generate the log-normal values by first deriving the mean and variance as shown and then standardizing this using,

$$z = \frac{\ln x - \alpha}{\beta} \tag{4}$$

This is similar to the normal distribution. So by choosing a range of values for z , we can generate a range of values for x. Fig. 3.1 illustrates an example of log normal distribution with a mean of 56.4 and different variances.

We have shown earlier that aperture values obey a log normal distribution, which is characterized by two parameters: the mean aperture and the standard deviation. In addition to the aperture density distribution parameters, the spatial correlation length and its anisotropy ratio for the variable apertures are needed to fully define the fracture.

The tail of the frequency distribution plays an important part since flow tends to occur preferred paths having the highest aperture distributions. Having distributed the apertures over a few points on the surface of the fracture, we move on to a Variogram to model the

relationship between the points and then to kriging to estimate the aperture values at points of no sampling.

3.4 Sampling and Estimation - Variogram and Kriging

The variogram is used by most geostatistical mapping and modeling algorithms. Conservatively, 80% of all geostatistical reservoir-modeling studies involve the use of the variogram for building one or all of the facies, porosity, and permeability models. Not only is the variogram used extensively, it has a great effect on predictions of flow behavior. The flow character of a model with a very short range of correlation is quite different from a model with a long range of correlation. Occasionally there are enough well data to control the appearance and flow behavior of the numerical models. The available well data are too widely spaced to provide effective control on the numerical model. The variogram provides the only effective control on the resulting numerical models. The lack of data, which makes the variogram important, also makes it difficult to calculate, interpret and model a reliable variogram. Variogram modeling is important and the "details" often have a crucial impact on prediction of future reservoir performance.

Furthermore, the variogram reflects our understanding of the geometry and continuity of reservoir properties and can have an important effect on predicted flow behavior and consequent reservoir management decisions. The variogram has been defined in many books and technical papers. In words, the variogram is the expected squared difference between two data values separated by a distance vector.

3.4.1 Modeling a variogram:

Measurements are often taken at a number of locations and the relationship between observations at the various locations can be explored by variogram analysis. A variogram summarizes the relationship between differences in pairs of measurements and the distance of the corresponding points from each other.

3.4.2 Variogram Features:

The main features of a variogram are,

a - Nugget variance : when the variogram appears not to go through the origin.

b - Range : the distance between locations beyond which observations appear independent i.e. the variance no longer increases.

c - Sill : describes where the variogram develops a flat region, i.e. where the variance no longer increases.

There are several methods available in the industry to model variograms. Some of them are spherical, exponential , linear, gaussian etc.. For our research we have used spherical model to model the variogram. The effectiveness of other models was also tested but we choose to stick to the spherical model for consistency. The model was consistent with different variances involved in the calculations.

Spherical Model:

The spherical model is probably the most commonly used to model variograms with a sill.

The equation for the spherical variogram can be written as,

$$\gamma(h) = C_0\left[1.5\left(\frac{h}{a}\right) - 0.5\left(\frac{h}{a}\right)^3\right] \text{ for h <= a} \quad (5)$$

$$= \quad C_0 \quad \text{for h > a} \quad (6)$$

3.4.3 Kriging

Kriging is based on the assumption that the parameter being interpolated can be treated as a regionalized variable. A regionalized variable is intermediate between a truly random variable and a completely deterministic variable in that it varies in a continuous manner from one location to the next and therefore points that are near each other have a certain degree of spatial correlation, but points that are widely separated are statistically independent. Kriging is a set of linear regression routines, which minimize estimation variance from a predefined covariance model. There are several types of kriging like

simple kriging, ordinary kriging, universal kriging, zonal kriging and indicator kriging. For our research purposes we have used ordinary kriging.

3.4.4 Generation of fracture aperture map from kriging

Earlier it was shown that by varying the values of normal variable z, generation of random values for fracture apertures is possible. From the experiments, we had shown that the fracture aperture width could be calculated from the single fracture flow experiments by assuming the cubic law. Utilizing the mean fracture aperture width calculated at different overburden pressures and assumed variances it was possible to generate random values for fracture apertures. This was achieved by varying the range of z from –2 to +2.

After generating sufficient number of aperture values (64 in all cases), the data was used to model the variogram to generate the model parameters nugget, sill and range. We used spherical fit to derive these parameters. We have kept lag distance as a constraint to effect consistency in our results. Figs. 3.4, 3.5 and 3.6 show the variogram modeling of the data for the various cases of overburden pressure. The mean fracture apertures determined from the experiments at overburden pressures of 500, 1000, 1500 was 56.4 μm, 40 μm , 20 μm respectively. The variance assumed for these three aperture widths were 200, 100 and 30 respectively.

Once the parameters are known we proceed to find the values of apertures at unsampled locations using kriging. The distance of interpolation corresponds to the size of the grid in the simulator. Figs. 3.7, 3.8, and 3.9 show the fracture aperture distribution maps generated through kriging. The aperture maps are the half widths of the actual. The maps generated through kriging may not represent the actual surface, but it is effective in imitating the surface of the fracture.

Having created the aperture maps through geostatistic modeling, our next step was to input the varying permeability layer corresponding to the aperture distribution into the simulation model to effectively study the flow through fractures.

3.5 Modeling fracture flow experiments

As pointed out earlier, modeling of flow experiments has posed a major challenge to the ongoing research on naturally fractured reservoirs. Tsang et al (1989) simulated similar flow experiments by generating a fracture aperture distribution and then with constant head boundary conditions on two opposite sides of the two-dimensional flow region, with closed boundaries on the remaining sides. The results show that the majority of flow tends to coalesce into certain preferred flow paths (channels), which offer least resistance. Tracer transport was also simulated using a particle tracking method. Tsang and Tsang (1990) chose a statistical description of a fracture with variable apertures by means of three parameters, performed numerical flow and transport experiments with them with particular emphasis of correlate the fracture geometry parameters. But concluded that the correspondence between observations and the hydrological properties is still ambiguous.

None of the literature in the past points to a case where experimental results were matched with particular reference to "real" fracture surfaces and the effect of surface roughness in the form of the "friction factor". Here we extend their methodology by analyzing the laboratory data and using it for generating a fracture aperture distribution with the aid of stochastic analysis, taking into consideration the effect of roughness on flow.

3.5.1 Simulation model:

In this study it was imperative to show that the cubic law fails when the fracture is modeled as smooth parallel plates. Figs. 3.10 and 3.11 show that by modeling the same, a match for flow rate and pressure drop could not be achieved. Also if one variable could be matched by altering the other, a simultaneous match could not be realized.

After a fracture aperture map was generated, we proceed to model the flow experiments. A numerical model utilizing commercial simulator (CMG™) was used to study the fluid flow through fractures at different overburden pressures. The laboratory process in which the water was injected through the fracture was duplicated in this modeling effort. The cuboid grid block was applied to overcome the difficulty of modeling a cylindrical core

shape (Putra *et al*. [1999]). A single porosity model was chosen since it is easier to model a single fracture than a dual porosity model. The volume of the core was maintained constant.

3.5.2 Conversion from cylindrical model to cuboid model:

Cylindrical core:

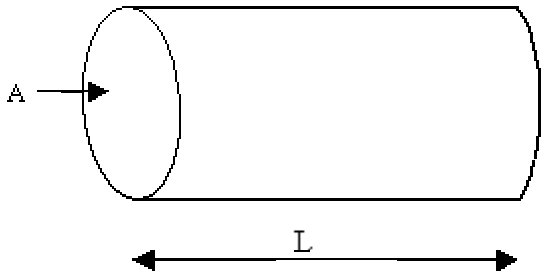

Core Specifications
Area (A) = 4.9637 Sq.cm
Diameter = 2.5146 cm
Length (L) = 4.9784 cm

Cuboid model for simulation:

Model Specifications
Height (h) = 1.9739 cm
Width (w) = 2.5146 cm
Length (L) = 4.9784 cm

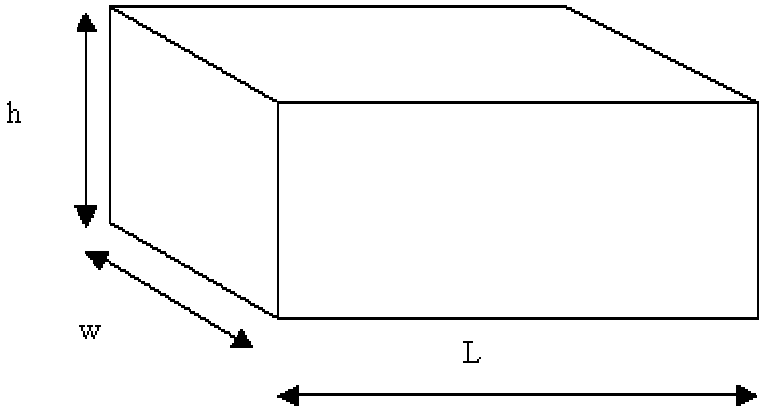

3.5.3 Establishing the correct model:

The first part of modeling any flow experiments is establishing the correct grid model that would enable the simulation of the experiments properly. We had two sets of data, one from the matrix flow experiments (unfractured core) and the other from fracture flow experiments (fractured core). In the first case flow experiments were conducted in an

unfractured core and the data from these experiments was used to establish an appropriate model, which would be utilized to simulate the fractured rock experiments. The data from unfractured core experiments is presented in Table 3.1.

The simulation model was first tested for grid sensitivity. The sensitivity studies showed that 31*15*15 was an optimum grid size. The results did not vary much when grid size was increased in the X or Y direction. It is imperative to first determine if the model is correct and efficient. We developed the model to simulate the matrix flow experiments. The results of the matrix flow experiments proved that the model was good enough to simulate the flow experiments. The model parameters are presented in Table 3.2.

The simulation run using this model gave impressive results. We were able to history match the results using the model. This ascertained the model and allowed us to carry forward the model for fracture flow experiments. Figures 3.12, 3.13, and 3.14 show the history matching for the matrix flow experiments for various overburden pressures and flow rates.

3.5.4 Surface Roughness Implications on Flow

The parallel plate model can be considered only a qualitative description of flow through real fractures. Real fracture surfaces are not smooth parallel plates, but are rough and contact each other at discrete points. Fluid is expected to take a tortuous path when moving through a real fracture. Thus deviations from the cubic law are expected. The experimental work by Iwai (1976) suggests that for rough-walled fractures under low normal stress, changes in the aperture result in changes in flow rate consistent with the cubic law. However, an electrical resistance analog by Tsang (1984) suggests that a 1-2 order magnitude error should result from neglecting the tortuosity when using the cubic law. We have attempted to explore and model the magnitude and nature of the disagreement between the parallel plate model and the actual flow through rough-walled fractures.

Several approaches have been used in the past that explicitly accounts for surface roughness. Various empirical flow laws have been presented that are based on

experiments with idealized geometry. One such experiment used parallel plates with sand glued to the walls to recreate small-scale roughness and another used parallel plates with various machining marks to recreate large-scale fractures (Iwai, 1976). There were many theoretical approaches that focused on redefining the cubic law to account for the surface roughness and the resulting tortuosity of the fluid flow paths.

Most of the previous studies have targeted the search for an appropriate definition of an average aperture in order to fit the cubic law. The general conclusion from these efforts is that the cubic law is valid when an average aperture can be defined. Many definitions of average aperture have been proposed, and for some reasons, some work better than others. Nonetheless, to date, these efforts have not converged to form a unified definition of the fracture aperture for the cubic law. In this research we have attempted to show that distributing the fracture and accounting for the friction due to the effect of surface roughness can effectively model the average aperture obtained from cubic law.

3.6 Our Approach

In order to effectively model the flow through fractures, we carefully observe the effect of surface roughness on flow. Since the surface of the fracture is rough, the roughness has to have an impact on the nature and magnitude of flow. The flow velocity is reduced because of the friction associated with it. Hence there is a decrease in flow rate when flow occurs through rough surfaces. In an experimental study of flow between sand-coated plates Lomize (1951) found that the friction factor could be generalized through the empirical relation given below.

$$f = 1 + 17\,(\in/D_h)^{1.5} \qquad \text{when } (\in/D_h) > 0.033 \qquad (7)$$

and

$$f = 1 \qquad \text{when } (\in/D_h) < 0.033 \qquad (8)$$

where the term $(\in/D_h)$ is known as the relative roughness.

Louis(1969) through a similar experiment showed that flow could be made to fit the experimental data by introducing a friction factor,

$f = 1 + 8.8\,(\in/D_h)^{1.5}$ when $(\in/D_h) > 0.033$ (9)

and

$f = 1$ when $(\in/D_h) < 0.033$ (10)

Both of these relations have been researched and we have found that both of them fit the data modeled by researchers in the past. For our purpose we have used Loius' empirical relation to fit our experimental data. The methodology will be discussed in the subsequent paragraphs.

3.6.1 Relative roughness:

In our research the relative roughness is calculated by taking ratio of the average roughness value over the hydraulic aperture of the fracture $(\in/D_h)$. The hydraulic aperture is given by the definition $D_h = 2^* 2b$, where 2b is the fracture aperture width. Figure 3.15 illustrates the concept of relative roughness.

Modification of permeability

After generating the fracture aperture distribution, we account for the effect of surface roughness by modifying the permeability distribution in the fracture surface. We achieved this by using the equation shown below.

$$k_f = \left(\frac{1}{f}\right) 8.45\times10^9\, w^2 \quad (11)$$

where, w is a fracture width in centimeters and f is the friction factor given by Louis (1969). Figures 3.16 and 3.17 show the difference in permeability distribution before accounting for roughness and after accounting for roughness. Modification of the permeability layer proved to be the key while simulating the fracture flow later to match the two parameters, flow rate and pressure drop across the core.

3.6.2 Fracture flow modeling:

A 31x15 grid block size was used in the x and y directions with 15 layers in the z direction. The fracture layer was incorporated in the 8th layer and the rest are matrix

layers. The modified permeability layer was used for the fracture layer, while the matrix layers had a constant permeability obtained from experimental analysis. For the first phase of preliminary results the simulation model was run for the 5cc/min injection rate case. All the layers were injected with constant water injection of 5 cc/min through injection points located at one extreme end and penetrating through all the layers. At the opposite end two production points were located, one for the matrix layers and the other for the fracture layer to quantify the amount of water produced at those two points.

In the experimental process, the core is saturated with the water. Once water injection was started with constant rate, water was produced simultaneously. Then the water that was produced from both matrix and fracture layers at the end point was recorded. In the simulation, however, the initial water saturation condition is assumed zero. A few minutes after the injection was started, the flow rate was still in the transient condition and then reached a steady state condition at later time. At steady state condition, we recorded the amount of water produced from matrix and fracture. Similar simulation runs were performed for different overburden pressures.

3.7 Results and Discussions

By introducing the corresponding modified permeability layer for the fracture, the results obtained were quite impressive. The results matched very closely, opening the door to more ventures through this kind of modeling. Earlier we had shown that by using a parallel plate model the match was not possible. Though we could individually match flow rate by increasing the permeability, we could not match the pressure drop simultaneously. Using a fracture distribution model, we have made it possible to match the experimental results, with good correlation between the two. Figures 3.18 and 3.19 show the results of the history match using a fracture distribution model.

The sensitivity analysis of our model in terms of changing variance of the aperture distribution showed that as variance increased, the flow through fractures increased. This was in correspondence with the earlier theory that fracture flow tends to be in preferred paths, through highest apertures. The model also validates that the fact that the tail of the

aperture distribution largely dominates the flow (Neuzil and Tracy, 1981). Fig. 3.20 illustrates the behavior of the flow through fractures as a result of increased variance. Fig. 3.21 shows the corresponding behavior of the pressure drop across the core in terms of increased variance of the aperture distribution.

3.8 Conclusions

1. From the observations we propose that the fracture aperture needs to be distributed to accurately model the experimental results.
2. The effect of friction due to surface roughness needs to be taken into account while modeling.
3. There is an increased flow though fractures when the variance of the aperture distribution is increased. This reiterates the fact that tortuosity in fluid flow is a significant factor.
4. Though we have shown that the mean aperture obtained from the cubic law could be effectively modeled using the methodology we adopted, the value of the mean fracture aperture is only a close estimate. The correct value of the mean aperture can be obtained with high accuracy using an X-Ray CT Scan.
5. This methodology could be effectively utilized for large field scale modeling for fractured reservoirs, where still the practice of using a constant permeability layer to model fracture layer exists. We have shown here that though constant permeability layer could match the flow rate and pressure drop across the core individually, the possibility of it matching both simultaneously is very remote.

3.9 Future Work

The next part of our research is to test the validity of our method by physically measuring the aperture and its distribution using an X-Ray CT Scan.

We plan to conduct two–phase flow experiments through a single fracture and extend this methodology also to two-phase flow by also investigating the relative permeability data in fractures.

3.10 References

Brown, S.R.: " Fluid Flow Through Rock Joints; The Effect of Surface Roughness," *Journal of Geophysical Research*, **92** (1987), No. B2,1,337-1,347.

Ge, S.: ' A governing equation for fluid flow in rough fractures," *Water Resources Research*, **33** (1997), 53-61.

Iwai, K.,: " Fundamental studies of fluid flow through a single fracture," Ph.D. thesis (1976), Univ. of Calif. Berkeley, CA.

Moreno, L., Y.W. Tsang, C.F. Tsang, F.V. Hale, and I. Neretnieks,.: "Flow and Tracer Transport in a Single Fracture : A Stochastic Model and Its Relation to Some Field Observations," *Water Resources Research*, **24** (1988) , No. 12, 2033-2048.

Neuzil, C.E., and Tracy, J.V.: "Flow Through Fractures,'" *Water Resources Research*, **17** (1981), No. 1, 191-199.

Putra, E., Fidra, Y., and Schechter, D.S.: "Study of Waterflooding Process in Naturally Fractured Reservoirs from Static and Dynamic Imbibition Experiments," paper SCA 9910 presented at the 1999 International Symposium of the Society of Core Analysts, Colorado, August 1-4.

Putra, E.: "Effect of Overburden Pressure on Unfractured and Fractured Permeability Cores," Semi-Annual Report (DOE Contract No.: DE-FC26-01BC15361), Oct 2001-March 2002.

Rossen, W. R. and Kumar, A. T. A.: "Single- and two-phase flow in natural fractures," paper SPE-24195 presented at the 1992 *Annual Technical Conference of the Society of Petroleum Engineers*, Washington, D. C.

Tsang, Y.W., Tsang, C.F., Neretnieks, I., Moreno, L.: " Flow and Transport in Fractured Media: A Variable Aperture Channel Model and Its Properties," *Water Resources Research*, **24** (1988), No. 12, 2-049-2,060.

Tsang, Y.W. and Tsang, C.F.: " Flow Channeling in a Single Fracture as a Two-Dimensional Strongly Heterogeneous Permeable Medium," *Water Resources Research*, **25** (1989), No. 9, pp. 2,076-2,080.

Tsang, Y.W. and Witherspoon, P.A.: 'The Dependence of Fracture Mechanical and Fluid Flow Properties on Fracture Roughness and Sample Size," *Journal of Geophysical Research*, **88** (1983), No. 3, 2359-2366.

Tsang, Y.W. and Tsang, C.F.: "Channel Model of Flow Through Fractured Media," *Water Resources Research*, **23 (**1987), No. 3, 467-479.

Tsang, Y.W., Tsang, C.F., Neretnieks, I., Moreno, L.: "Flow and Tracer Transport in Fractured Media : A Variable Aperture Channel Model and Its Properties," *Water Resources Research*, **24** (1988), No. 12, 2049-2060.

Zimmerman R.W. and Bodvarsson, G.S.: "Hydraulic Conductivity of Rock Fractures" *Transport in Porous Media*, **23**, 1-30 (1996).

Witherspoon, P. A., Wang, J. S. Y., Iwai, K. and Gale, J. E.: "Validity of cubic law for fluid flow in a deformable rock fracture, *Water Resources Research*, **16** (1980), No. 6, 1016-1024.

Table 3.1 - Matrix flow experimental observations

Injection rate, cc/min	Over burden pressure, psia	Pressure drop, psia
5 cc	500	4.1
5 cc	1000	4.5
5 cc	1500	5.1
10 cc	500	8.1
10 cc	1000	9.35
10 cc	1500	10.8
15 cc	500	12.4
15 cc	1000	13.7
15 cc	1500	16.4

Table 3.2 - Simulation model parameters

Grid	31*15*15
Porosity	0.2358
Pore Volume	5.827 cc
Water Density	1 g/cc
Compressibility	5.19295E-07 (1/psi)
Viscosity	1 cp
Reference pressure	7929.97 psia
Rock compressibility	4.35113E-07 (1/psi)

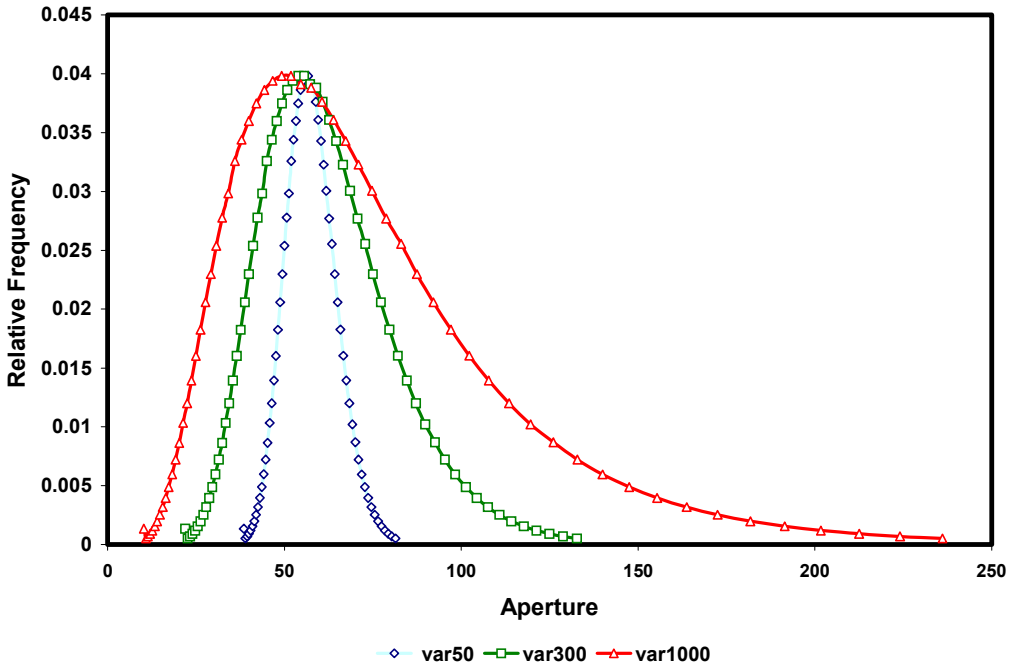

Fig. 3.1 - Example of lognormal distribution for different variance

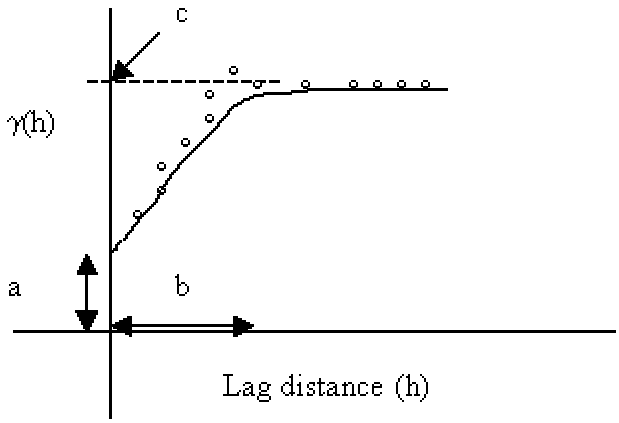

Fig. 3.2 - Features of a variogram.

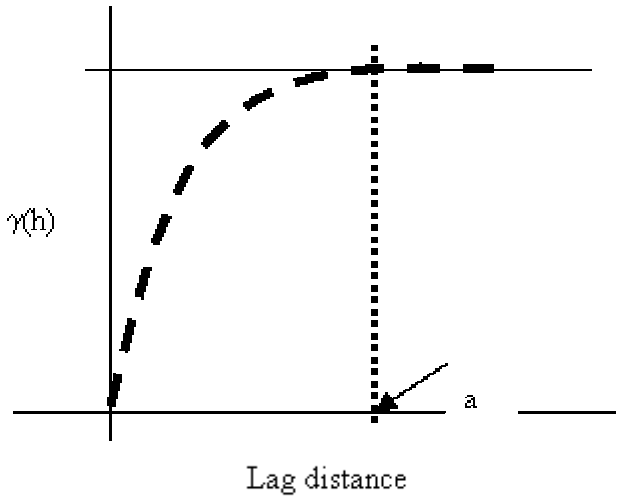

Fig. 3.3 - Spherical modeling of variogram

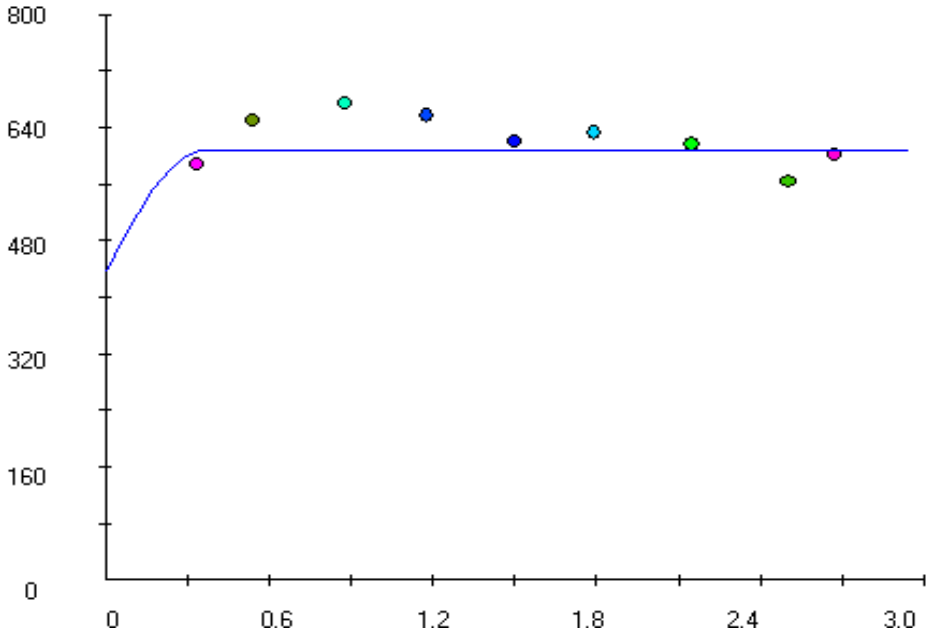

Fig. 3.4 - Variogram modeling for mean aperture = 56.4 μm variance = 200

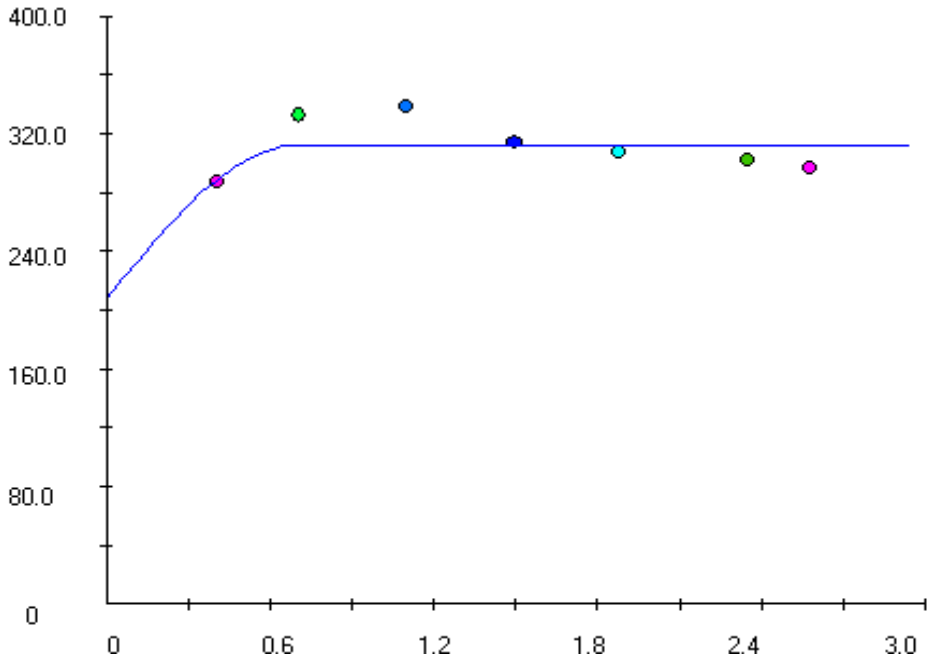

Fig. 3.5 - Variogram modeling for mean aperture = 40 μm variance = 100

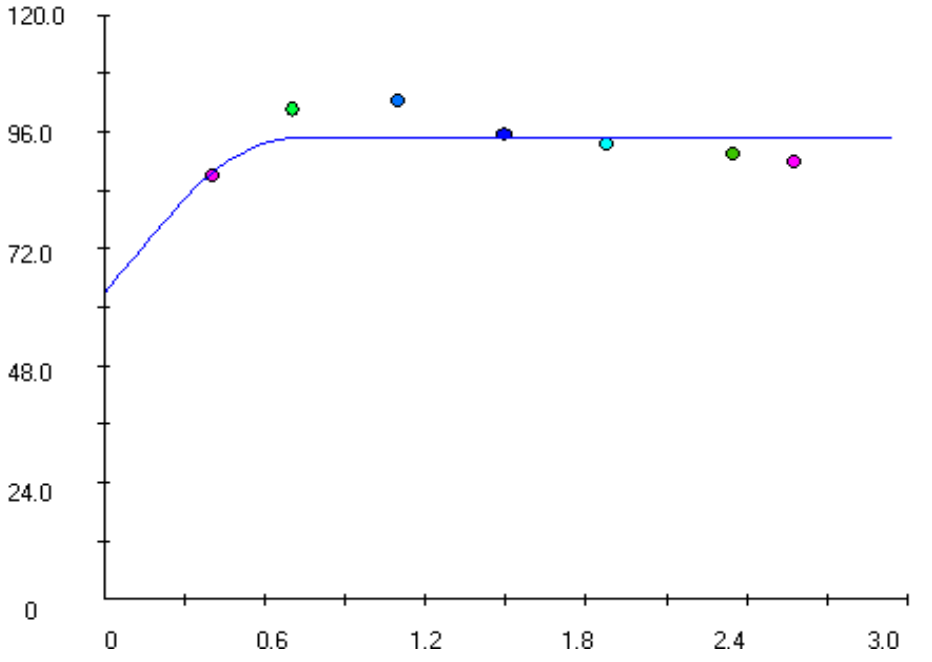

Fig.3.6 - Variogram modeling for mean aperture = 30 μm variance = 30

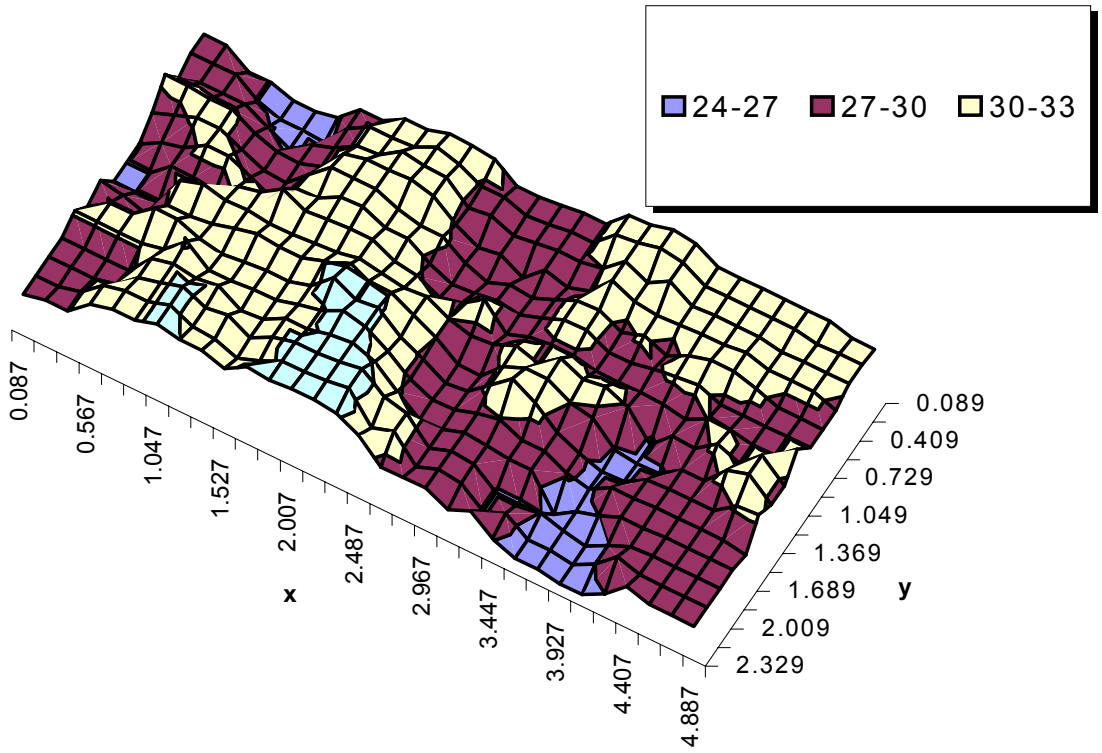

Fig. 3.7 - Kriged fracture aperture map for mean width = 56.4 μm and variance = 200

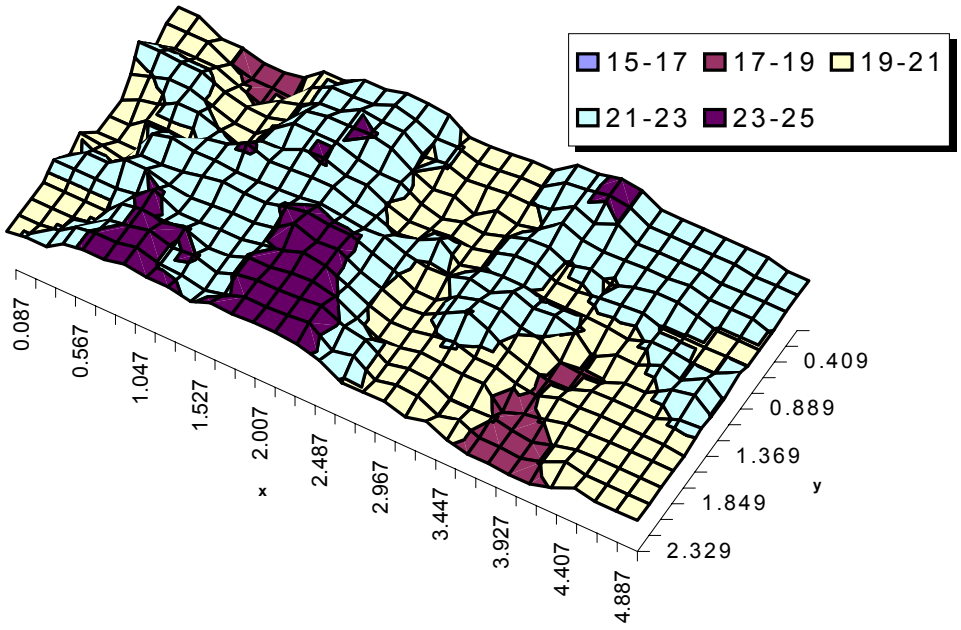

Fig. 3.8 - Kriged fracture aperture map for mean width = 40 μm and variance = 100

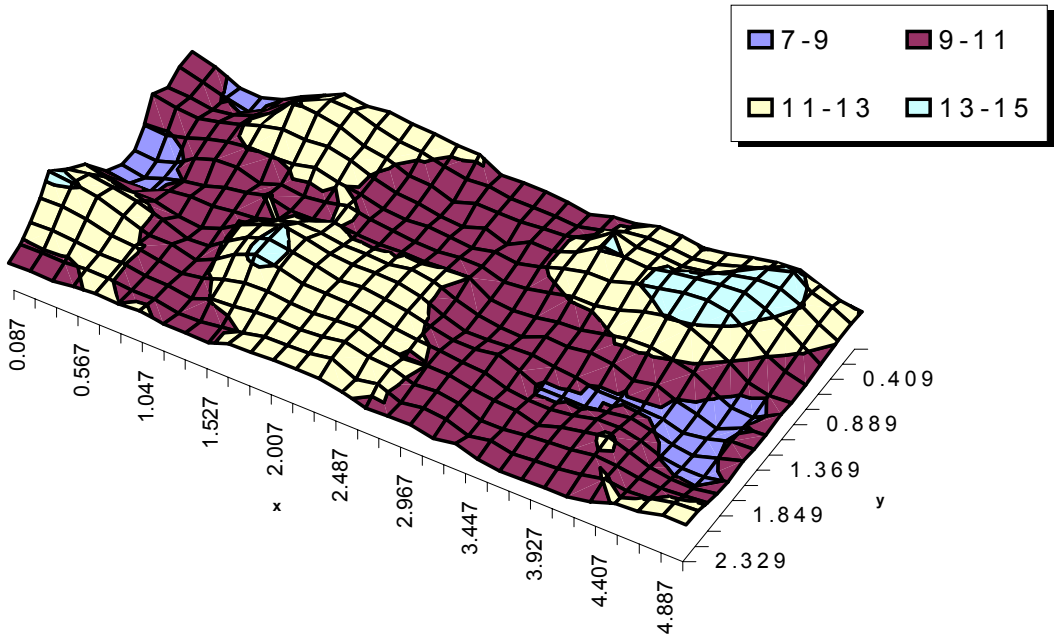

Fig. 3.9 - Kriged fracture aperture map for mean width = 20 μm and variance = 30.

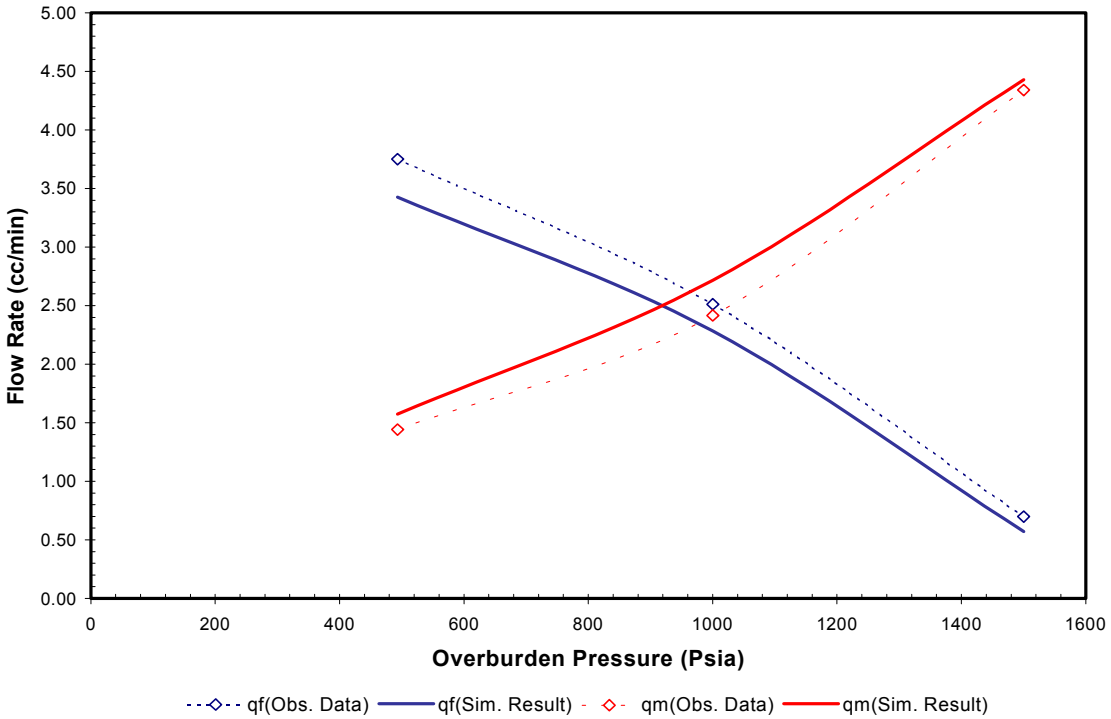

Fig. 3.10 – The flow rates comparison between laboratory and simulation results at 5 cc/min at different overburden pressures.

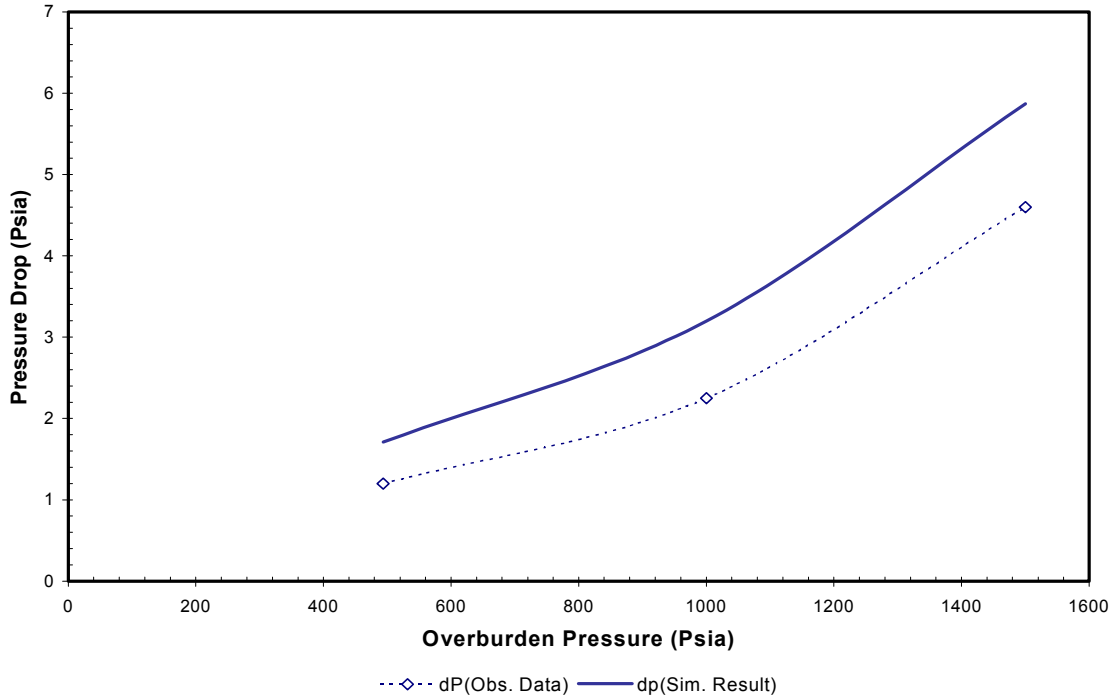

Fig. 3.11 – The pressure drop comparison between laboratory and simulation results at 5 cc/min and at different overburden pressures.

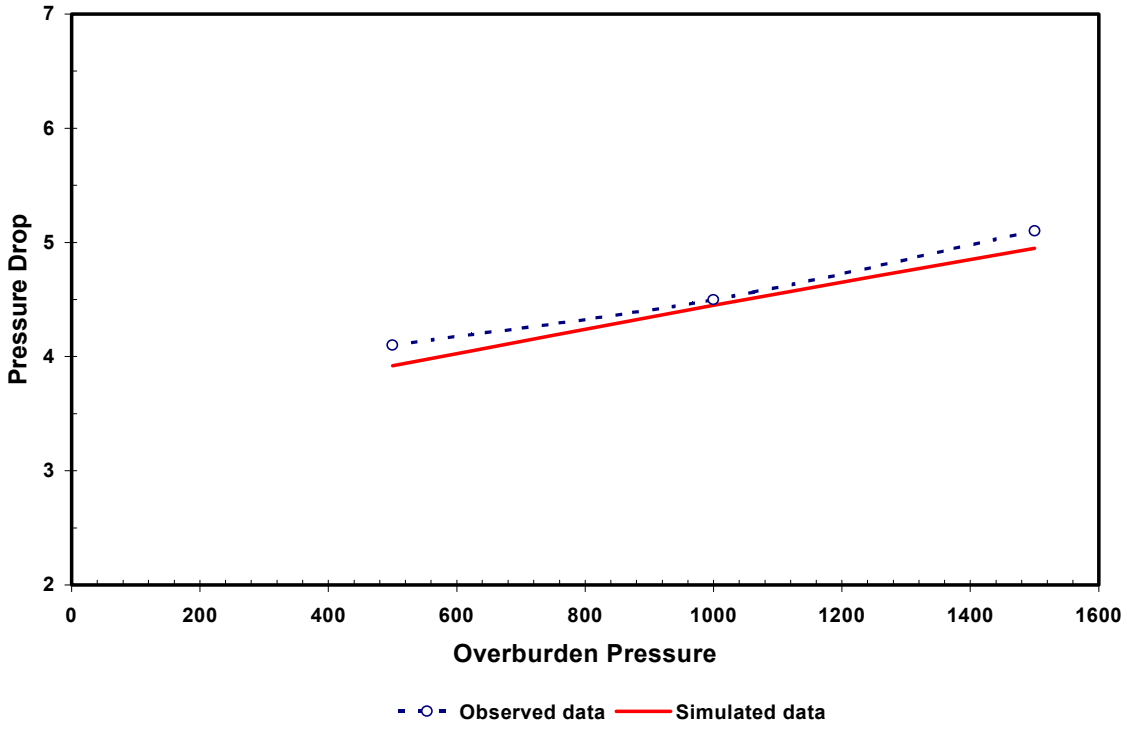

Fig.3.12 - History matching of matrix flow experimental data for q= 5 cc/min.

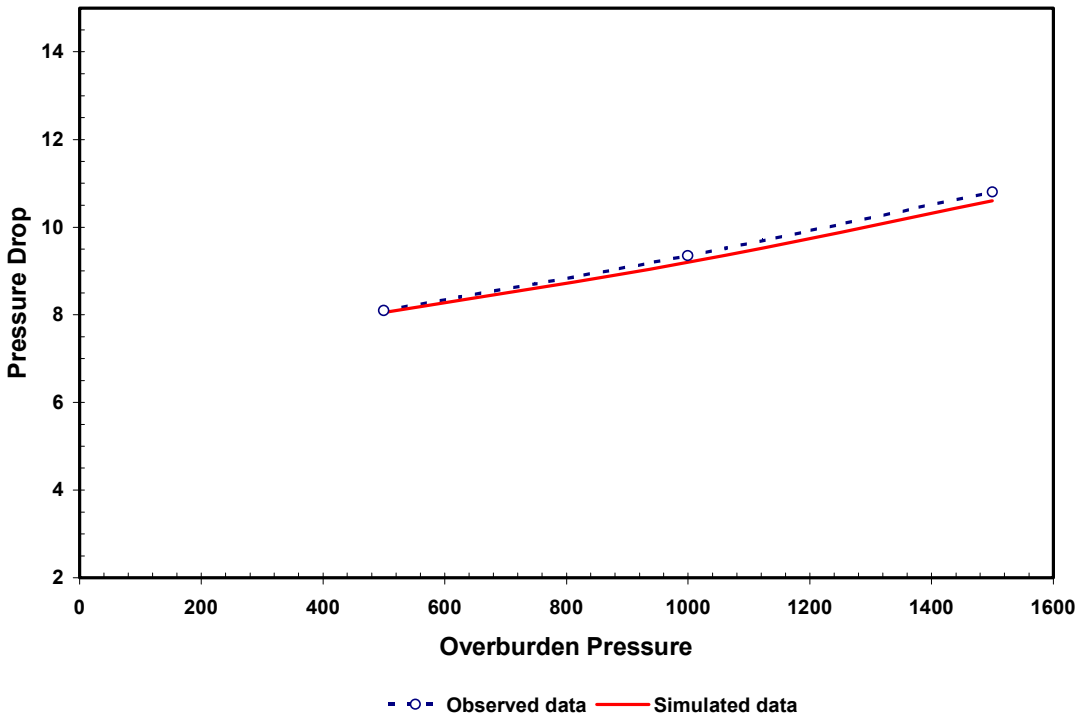

Fig. 3.13 - History matching of matrix flow experimental data for q= 10 cc/min

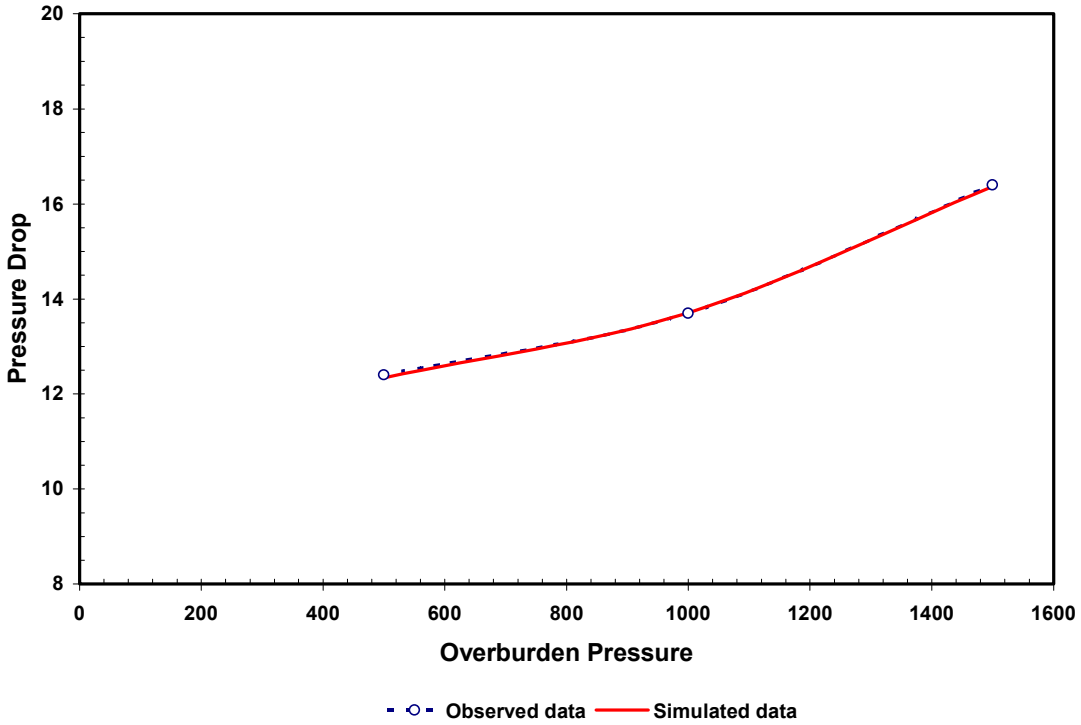

Fig. 3.14 - History matching of matrix flow experimental data for q= 15 cc/min

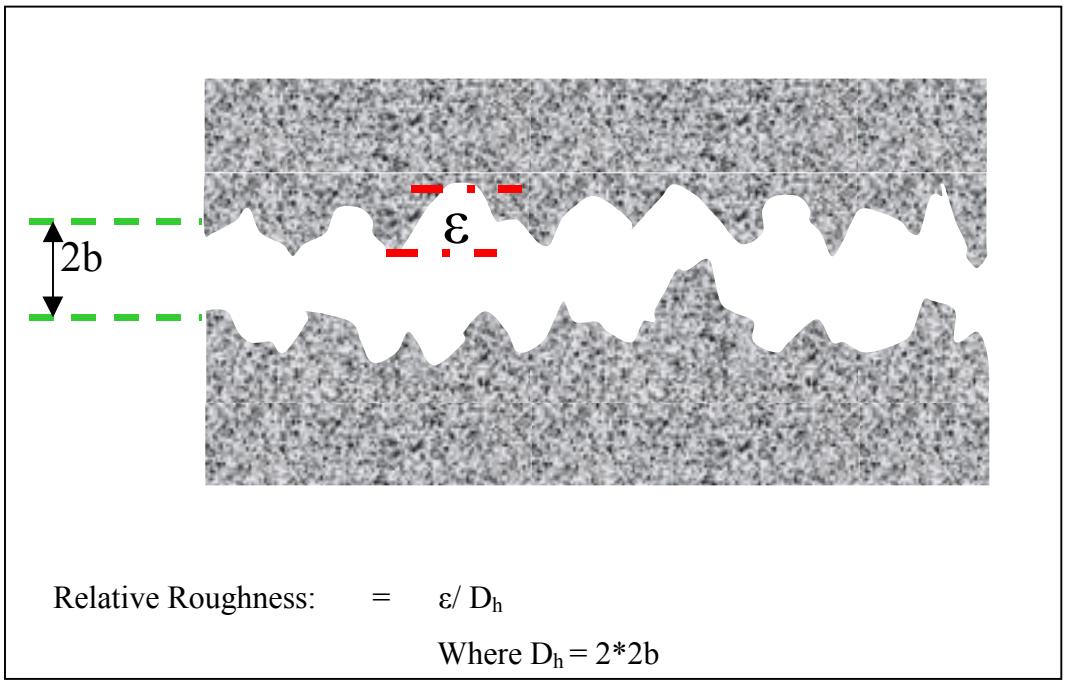

Fig. 3.15 - Relative roughness

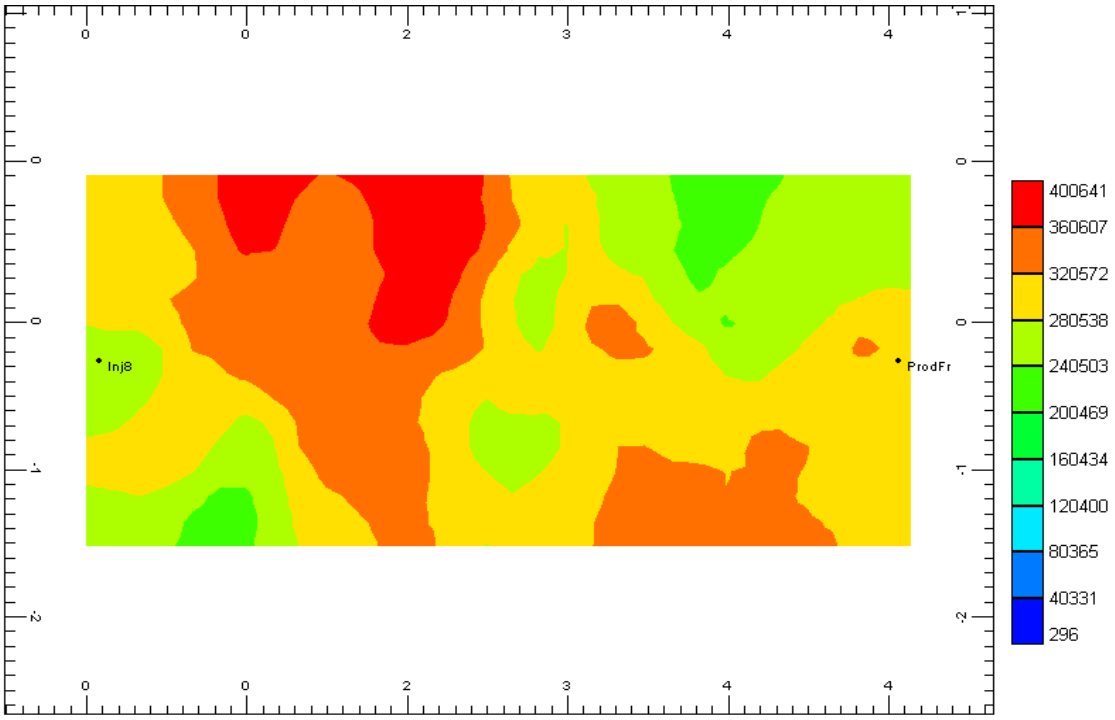

Fig. 3.16 - Fracture permeability distribution before accounted for surface roughness

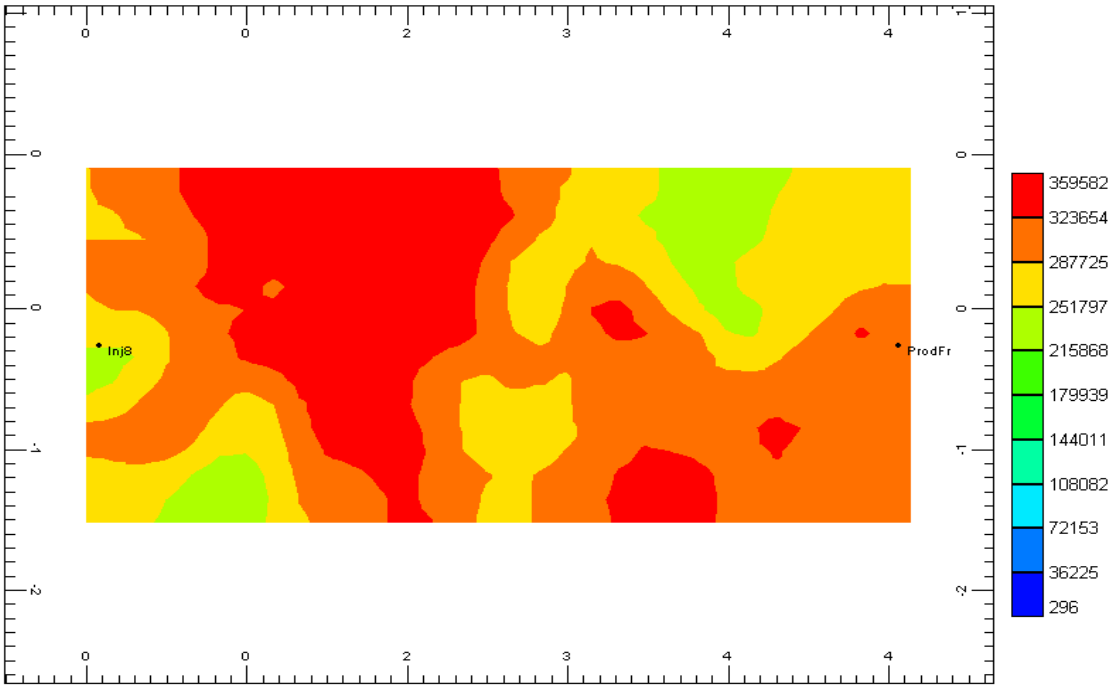

Fig. 3.17 - Fracture permeability distribution after accounted for surface roughness

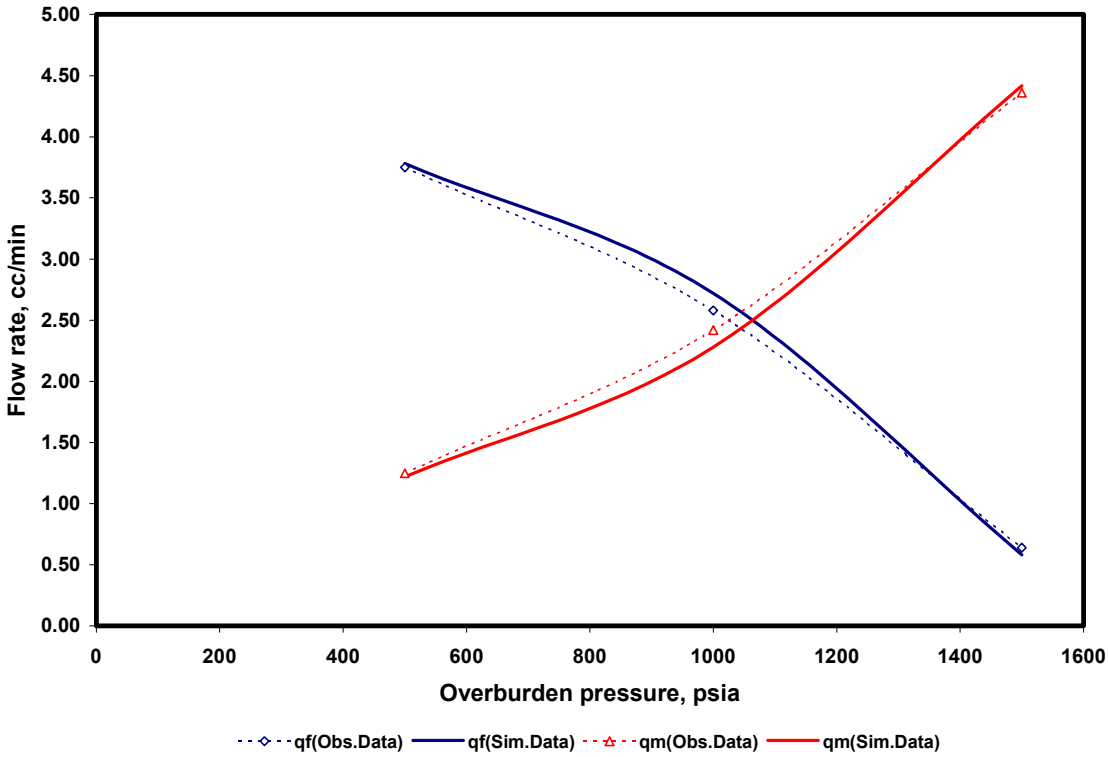

Fig. 3.18 - The flow rates comparison between laboratory and simulation results at 5 cc/min and at different overburden pressures.

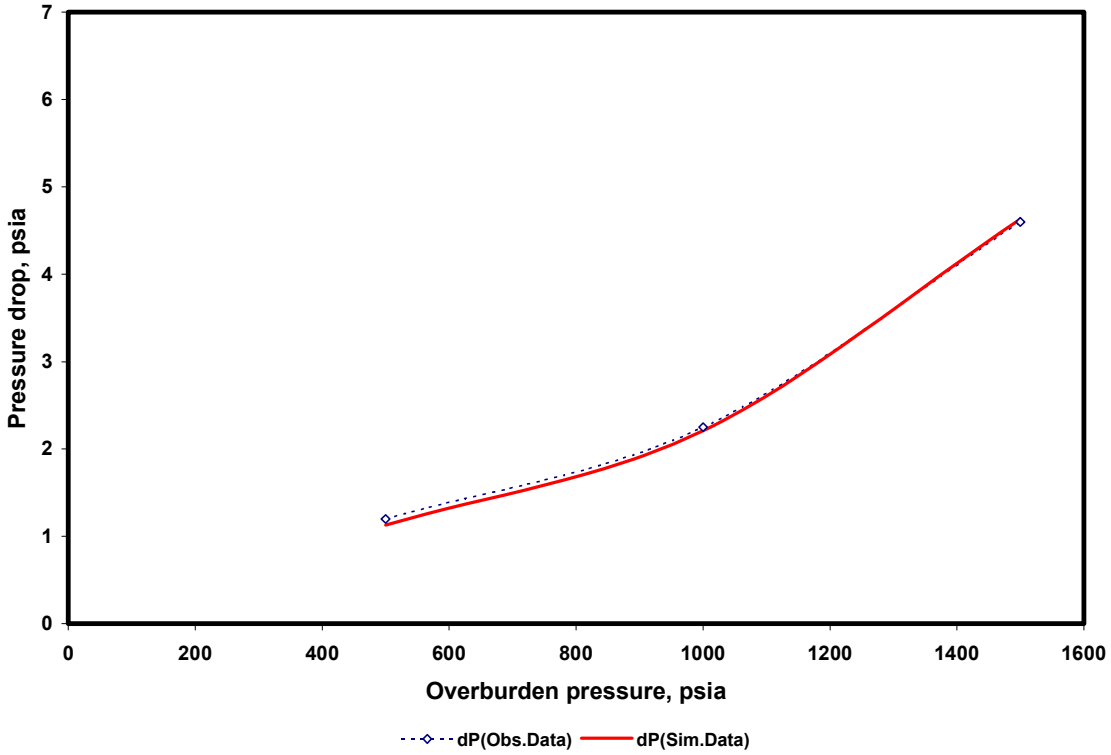

Fig. 3.19 – The pressure drop comparison between laboratory and simulation results at 5 cc/min and at different overburden pressures.

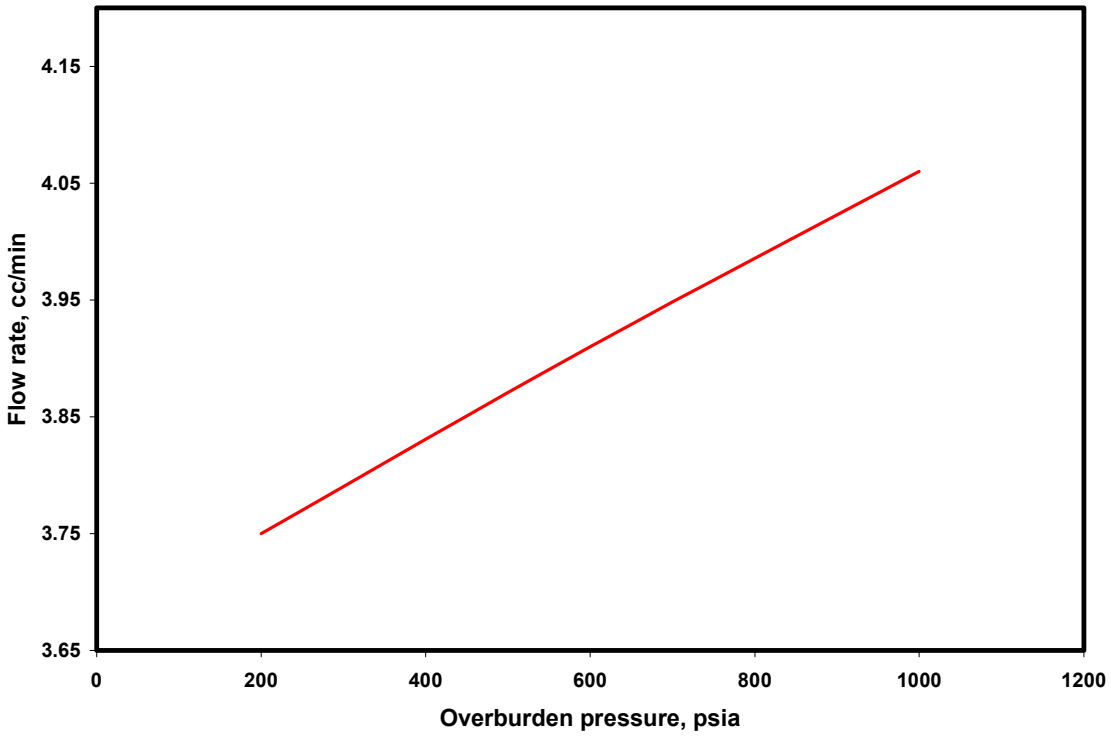

Fig. 3.20 - Effect of changing variance of aperture distribution on flow through fracture

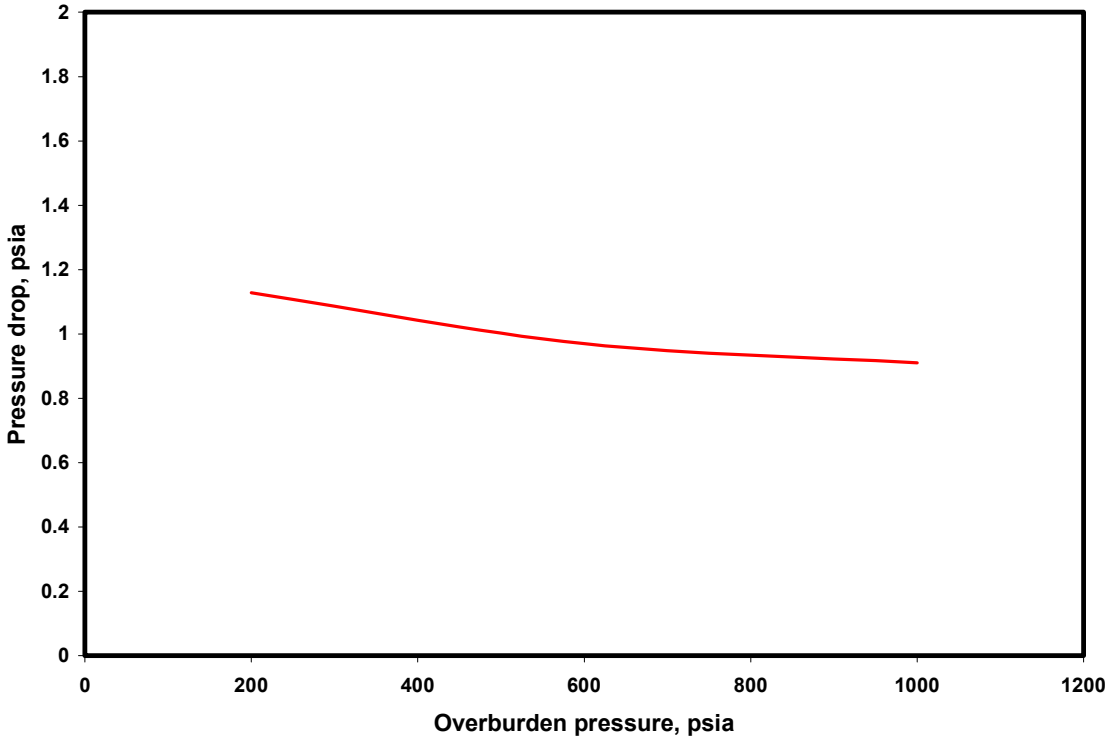

Fig. 3.21 - Effect of changing variance of aperture distribution on pressure drop across fracture